

High-order Knowledge Based Network Controllability Robustness Prediction: A Hypergraph Neural Network Approach

Shibing Mo, Jiarui Zhang[†], Jiayu Xie[†], Xiangyi Teng^{*}, *Member, IEEE*, and Jing Liu, *Senior Member, IEEE*

Abstract—In order to evaluate the invulnerability of networks against various types of attacks and provide the guidance for potential performance enhancement as well as controllability maintenance, network controllability robustness (NCR) has attracted increasing attention in recent years. Traditionally, the controllability robustness is determined by attack simulations, which is computationally time consuming and only applicable for small-scale networks. Although some machine learning based methods for predicting network controllability robustness have been proposed lately, they only focus on pairwise interactions of complex networks and the underlying relationships between high-order structural information and network controllability robustness are not explored. In this paper, a dual hypergraph attention neural network model based on high-order knowledge (NCR-HoK) is proposed to accomplish the tasks of robustness learning and controllability robustness curve prediction. Through the proposed node feature encoder, the construction of hypergraph with high-order relation and dedicatedly designed dual hypergraph attention module, our method can effectively learn three types of network information simultaneously: the explicit structural information in the original graph, the high-order connection information in local neighborhoods and more hidden features in the embedding space. Notably, we explore for the first time the impact of high-order knowledge on the network's controllable robustness. Compared to the state-of-the-art methods for network robustness learning, our method has superior performance on both synthetic and real-world networks with low overheads.

Index Terms—Complex network, hypergraph, controllability, graph attention neural network, controllability learning.

I. INTRODUCTION

COMPLEX network is an interdisciplinary subject covering computational mathematics, physics, computer, biology, and other fields [1]–[4]. Nowadays, researches on complex network can help us analyze the composition of large-scale systems, the operating dynamics of network members and the

distribution rules of functional structures. Therefore, network science has received enormous attention in recent years [5]–[8]. Generally, systems with different structures undertake different types of tasks and inevitably will face complicated and changeable application scenarios. Various external factors such as natural disasters or man-made attacks could interfere with the normal operation of the system [9]. Under such circumstances, a robust network needs to maintain relatively stable functions even when it suffers certain attacks or damage [10]. In order to evaluate the invulnerability or controllable capacity of different networks and provide a reasonable reference for potential performance enhancement, network controllability robustness has become one of the core issues in the field of network science [11]–[15].

Generally speaking, the measure of the network controllability robustness is quantified by a sequence of values that record the remaining controllability of the network after a sequence of attacks [16]–[19]. Here, the attacks can be divided into random attack or malicious attack. The former means that the attacker randomly selects targets from the network to attack, and the latter indicating that the attacker targets the most important members (nodes or edges) of the current network. For a random network, the distribution of the significance of network members follows Poisson distribution; that is, the importance of each node is similar and there are no apparent key nodes. Therefore, random attacks are relatively more destructive to this kind of network since random network has strong tolerance for malicious attacks [20]. For scale-free networks, the distribution of network members exhibits a power law distribution characteristic; that is, very few nodes are critical and need to be highly protected. This makes the network very vulnerable to malicious attacks but robust to random attacks [21].

Although the correlation between local topological structure and network controllability has been investigated during last decades, there is no systematic study on underlying relationships between high-order structural information and network controllability robustness. Existing methods often rely on measures like degree and betweenness [22], [23] or focus on pairwise interactions and local structures such as rings and chains [24]–[26]. While insightful, these approaches largely overlook crucial high-order connection information, where multiple nodes might interact collectively or share complex dependencies which are not captured by simple dyadic relationships. This issue is significant because such multi-way interactions, representing functional groups, community

This work was supported in part by the National Natural Science Foundation of China under Grant 62306224 and Grant 62471371, in part by the Guangdong Highlevel Innovation Research Institution Project under Grant 2021B0909050008, in part by the Guangzhou Key Research and Development Program under Grant 202206030003 and in part by the Fundamental Research Funds for the Central Universities under Grant YJSJ25014.

Shibing Mo, Jiarui Zhang and Jing Liu are with the School of Artificial Intelligence, Xidian University, Xian 710126, China. Jiayu Xie is with the School of Computer Science and Technology, Xidian University, Xian 710126, China. Xiangyi Teng is with the Guangzhou Institute of Technology, Xidian University, Guangzhou 510555, China.

Email: msb@stu.xidian.edu.cn; 2901999089@qq.com; 3630729140@qq.com; tengxiangyi@xidian.edu.cn; neouma@mail.xidian.edu.cn.

Xiangyi Teng is the corresponding author.

Authors marked with [†] contributed equally to this work.

The source code and supplementary materials for our work are available at <https://github.com/Explorermomo/NCR-HoK>.

structures, or complex influence pathways, are hypothesized to fundamentally affect how a network's controllability responds to perturbations. To address this challenge, the introduction of hypergraph is a promising solution. Unlike traditional graphs, hypergraphs employ hyperedges that can connect any number of nodes, offering a more expressive framework to naturally model these many-body interactions and capture a richer understanding of the network's intricate organization, which we believe is key to more accurately assessing controllability robustness.

Traditionally, the controllability robustness is determined by attack simulation, which is computationally time consuming. Lately, some machine learning based methods for predicting network controllability robustness have been proposed. In [27] and [28], the convolutional neural network (CNN) based predictor for controllability robustness (PCR) and a knowledge-based predictor for controllability robustness (iPCR) are proposed, which achieve high-precision controllability robustness learning when the training and test sets maintain the same distribution. In [29], the authors proposed to learn network robustness via Low-Complexity spectral graph neural networks. However, these methods, while innovative, also tend to dismiss the impact of underlying high-order structural information and can be challenging to train due to their high complexity (e.g., iPCR), making them less practical for large-scale networks.

To overcome these limitations and effectively integrate high-order structural insights, this paper introduces a graph attention neural network model based on high-order knowledge (NCR-HoK). We explicitly construct hypergraphs from the input network to capture this vital high-order information. Specifically, we employ methods such as K-hop neighborhood analysis and K-Nearest Neighbors (K-NN) for hypergraph construction due to their ability to reveal distinct aspects of network topology. The motivation and main contributions of our paper are as follows:

- The K-hop approach defines hyperedges by encompassing nodes within a specific path distance (K hops). This is motivated by the understanding that a node's influence and its contribution to overall network controllability often extend beyond its immediate connections, and capturing these extended local environments as single hypergraph structures can reveal how local clusters collectively impact robustness.
- The K-NN method, typically applied to node embeddings or structural feature vectors, groups nodes that exhibit similar topological roles or characteristics, even if not directly linked. Hyperedges formed from such K-NN groups can uncover latent communities or functionally related node sets whose collective behavior underpins network stability.
- By leveraging these diverse hypergraph construction strategies, we aim to extract multifaceted high-order structural data. This rich high-order knowledge, embedded within the hypergraph, is then processed by our NCR-HoK model. The attention mechanism within this model is particularly well-suited to learn and weigh the significance of these complex multi-node interactions and high-order patterns for the tasks of robustness learning and controllability

robustness curve prediction.

- Compared to traditional network attack simulation-based methods and cutting-edge machine learning methods, the proposed NCR-HoK aims to consume significantly less time to obtain an accurate controllability robustness measurement for different types of real-world and synthetic networks, with lower overheads in training.

In summary, the core contribution of NCR-HoK lies in designing a novel hypergraph-based model, which is the first to integrate K-hop/K-NN hypergraph construction with a dual-channel attention mechanism. Through comprehensive experimental and theoretical analysis, it is demonstrated that NCR-HoK can fully extract high-order knowledge from networks, thereby enabling the accurate prediction of controllable robustness curves for networks.

The remainder of this article is organized as follows. Section II reviews the research of network controllability and controllability robustness against various attacks. Section III provides preliminary and basic knowledge for the proposed method. Section IV describes how HCR-HoK works in detail. In Section V, extensive experimental studies are conducted with comprehensive analysis. Finally, Section VI concludes the whole paper. The supplemental materials are given in Section VII and can be downloaded along with this article.

II. RELATED WORK

A. Network Controllability Robustness Predictors

In the last few years, some machine learning based methods for predicting network controllability robustness have been proposed to address the limitation of traditional simulation-based methods. Among them, PCR [27] is a predictor based on a single CNN. This framework transforms complex network data into grayscale images, typically by using the adjacency matrix as input to the CNN. iPCR [28] is an improved version of PCR, employing a set of CNNs to predict network controllability robustness. This approach leverages a large amount of simulation-generated training data to train the ensemble of CNNs, which are used for both classification and regression tasks. iPCR outperforms the classical single-CNN predictor in terms of prediction accuracy, and it also achieves better performance than traditional spectral metrics and network heterogeneity measures. Recently, several graph neural network(GNN) based methods have also been proposed. [30] introduced a graph convolutional network(GCN) model that directly takes network topology and node features as input, rather than converting them into grayscale images. Compared to CNN-based methods, this GCN model requires only 1% of the parameters, yet achieves better prediction performance across various synthetic networks and six real-world networks. [29] proposed a controllability robustness learning model based on a spectral graph neural network, named CRL-SGNN. This model first uses graph convolutional layers to generate network representations incorporating topological information and node degree centrality, and then employs a multi-branch prediction module to output robustness metrics.

However, these methods largely overlook critical high-order connectivity information. This issue is significant, as multi-

node interactions—representing functional groups, community structures, or complex influence paths—are believed to fundamentally affect how network controllability responds to perturbations.

B. Hypergraph Neural Network

A hypergraph is a generalization of a graph that introduces hyperedges, which can connect multiple nodes simultaneously, enabling the representation of high-order relationships. HGNNs [31] are designed to capture such high-order associations by employing hyperedge convolution or attention mechanisms, allowing node representations to incorporate high-order structural information. Compared to GCNs, HGNNs are capable of modeling latent structures in complex multimodal data and have demonstrated superior performance on tasks such as node classification and visual recognition. In recent years, various HGNN models have been developed. HGNN+ [32], for instance, is tailored for multimodal or heterogeneous data. It first constructs sets of hyperedges for each modality to represent latent high-order correlations. These modality-specific hypergraphs are then merged into a unified hypergraph via an adaptive fusion strategy, upon which spatial-domain convolution is applied. Besides, some approaches incorporate attention mechanisms to weigh the importance of different hyperedges. For example, the Hypergraph Attention Network [33] introduces attention coefficients between nodes and their associated hyperedges to enhance information filtering. DHHNN [34] combines the advantages of hyperbolic geometry, dynamic hypergraphs, and the self-attention mechanism to enhance multimodal data representation learning. [35] proposed the Dual-view HGNN, which constructs two sets of hyperedges from the topological structure and node attributes, respectively. It employs both shared and view-specific hypergraph convolutional layers—augmented with attention mechanisms—to deeply model the complex relationships among nodes. In summary, as a high-level form of graphical representation, hypergraphs find numerous applications in the field of graph data mining, as detailed in **Supplementary Materials VII. A**.

This paper proposes NCR-HoK, which captures high-order semantics from multiple perspectives by jointly leveraging the original feature space and the embedding space. The learnability and dynamic adaptability of the embedding space further enhance the model’s capacity to extract and integrate high-order information.

III. PRELIMINARIES

This section first introduces the concept and calculation of controllability robustness for a given complex network, which reflects the network system’s ability to maintain a controllable state. Then we discuss the concept of high-order hypergraph structures in complex networks. Finally, the error measurement and evaluation criteria used in this study for learning network controllability robustness are presented.

A. Network Controllability Robustness

The controllable robustness of complex networks reflects the ability of network systems to maintain or restore their

controllability at the lowest cost. For a linear time-invariant network system $\dot{x} = Ax + Bu$, where A and B are the transposed adjacency matrix and input matrix, and x and u are the state vector and input vector. The full rank of the controllability matrix $[B \ AB \ A^2B \ \dots \ A^{N-1}B]$ is a necessary and sufficient condition for state controllability, where N represents the dimension of A and the total number of nodes in the network. Based on the minimum input theorem [10], the minimum number of driver nodes N_D for a directed network can be determined by $N_D = \max\{N - |E^*|, 1\}$, where $|E^*|$ is the number of edges in the maximum matching E^* . For undirected networks, the minimum number of driver nodes N_D can be determined by $N_D = \max\{N - \text{rank}(A), 1\}$ according to the framework of exact controllability [9].

Then, the calculation of network controllable robustness is as follows:

$$n_D(i) = \frac{N_D(i)}{N - i}, i = 1, 2, \dots, N - 1 \quad (1)$$

where $N_D(i)$ is the number of driver nodes needed to retain the network controllability after removing i nodes, and $N - i$ is the number of remaining nodes after the i -th attack. By recording the controllable robustness of each state during a network attack, we can obtain a curve of the network’s controllable robustness, which intuitively reflects the changes in the network’s robustness throughout the attack process.

B. Hypergraph Representation Learning

A hypergraph is defined as $G_H = \{V, E, F\}$, where $V = \{v_1, v_2, \dots, v_N\}$ represents the set of nodes in the graph and $E = \{e_1, e_2, \dots, e_M\}$ represents the set of hyperedges. For any hyperedge, it can contain two or more nodes. It is worth noting that the topology of hyperedge G_H can be also represented by the association matrix $A_{H_{ij}} \in R^{N \times M}$, with entries defined as:

$$A_{H_{ij}} = \begin{cases} 1, & \text{if } v_i \in e_j \\ 0, & \text{if } v_i \notin e_j \end{cases} \quad (2)$$

In general, each node in the hypergraph can have a d -dimensional attribute vector. Therefore, all node attributes can be expressed as $F = [F_1, F_2, \dots, F_N]^T \in R^{N \times d}$.

Hypergraphs [31], [36]–[38] have attracted more and more attention in recent years. For mining hypergraph structures, [32] gives four generation methods, namely hyperedge group using pairwise edge, hyperedge group using k-Hop neighbors, hyperedge group using attributes, and hyperedge group using features. The generated hypergraph structures can effectively mine the high-order knowledge of graph structures and provide unique data analysis perspectives for downstream tasks such as recommender systems [39], text categorization [40], disease diagnosis [41], and chip layout wiring [42]. As for the controlled robustness analysis of complex networks, how to use hypergraphs and analyze the impact of high-order knowledge on network controlled robustness is an interesting research topic.

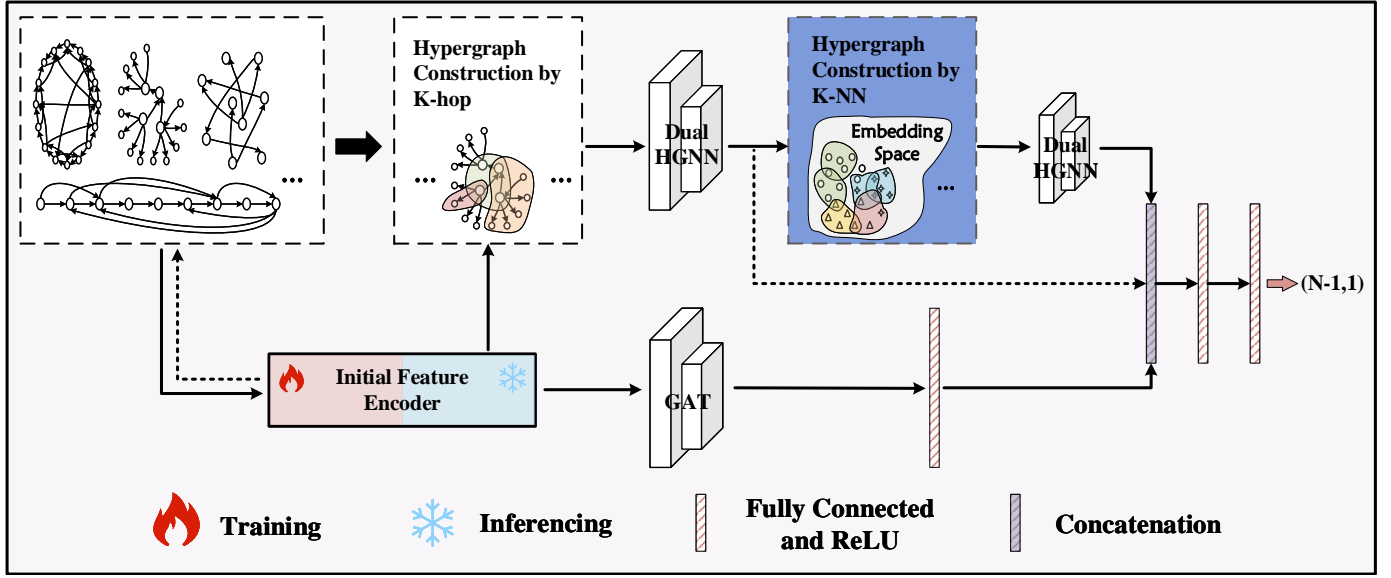


Fig. 1. The Overview of the proposed NCR-HoK framework. NCR-HoK can effectively learn three types of network information simultaneously: the explicit structural information in the original graph, the high-order connection information in local neighborhoods and more hidden structures and features in the embedding space.

C. Measurement of Network Controllability Robustness

This paper employs four types of curves to measure and describe the controllable robustness of networks. For M networks with the node size denoted as N , their true robustness profile is expressed as $tv \in R^{M \times (N-1)}$ and the robustness profile predicted by the model is expressed as $pv \in R^{M \times (N-1)}$. The four types of curves are introduced as follows: 1) The actual controllable robustness curve of the network $TC = \text{mean}(tv) \in R^{1 \times (N-1)}$, obtained through attack simulation methods combined with the formulas from references [9] or [10]. 2) The predicted controllable robustness curve $PC = \text{mean}(pv) \in R^{1 \times (N-1)}$. 3) The error curve between the predicted and actual values $er = \text{mean}(|pv - tv|) \in R^{1 \times (N-1)}$. 4) The standard deviation curve between the predicted and actual values $\sigma = \text{std}(|pv - tv|) \in R^{1 \times (N-1)}$.

In addition to analyzing relevant curve graphs, this article also utilizes two evaluation metrics, \bar{er} and $\bar{\sigma}$, where \bar{er} represents the mean accuracy of the model's predictions for controllable robustness curve and $\bar{\sigma}$ represents the average deviation in the accuracy of these predictions. For both \bar{er} and $\bar{\sigma}$, lower values indicate better performance, and the \bar{er} and $\bar{\sigma}$ are calculated as follows:

$$\bar{er} = \text{mean}(er) \in R \quad (3)$$

$$\bar{\sigma} = \text{mean}(\sigma) \in R \quad (4)$$

IV. PREDICTOR FOR NETWORK CONTROLLABILITY ROBUSTNESS

In this section, we construct high-order network structure using hypergraphs and introduce our model (NCR-HoK) that combines Attention Neural Networks to obtain high-order knowledge of graphs for predicting the controllable robustness curve of graphs. The overall framework of our model is shown in Fig.1. In NCR-HoK, the node feature encoder encodes

the in-degree, out-degree, and betweenness centrality of the graph to obtain initial node features. It integrates features of the graph structure using both the Graph Attention (GAT) Network and the Dual Hypergraph Attention (Dual HGNN) Network. Initially, the GAT network embeds the original graph structure to learn the explicit features of the graph. Subsequently, the Dual HGNN network embeds the generated hypergraph structure to learn hidden and high-order features of the graph. Additionally, the K-NN method adaptively generates hypergraphs in the embedding space of the graph. The Dual HGNN network then embeds these generated hypergraph structures to further explore the potential connections between the graph structure and the graph's controllable robustness curve. Detailed information about NCR-HoK is described below.

A. Node Initial Feature Encoder

In the study of controllable robustness of graphs, structural properties such as node in-degree, out-degree, and betweenness centrality play crucial roles. They provide deep insights into the structure and function of graphs, thereby influencing their performance in responding to external disturbances. Consequently, the node initial feature encoder of NCR-HoK encodes these aspects separately and then concatenates the results to obtain the initial features of the nodes.

The betweenness centrality of a node v is defined as:

$$C_B(v) = \sum_{s \neq v \neq t} \frac{Path_{st}(v)}{Path_{st}} \quad (5)$$

where $Path_{st}$ denotes the total number of shortest paths from node s to node t , and $Path_{st}(v)$ denotes the number of those paths that pass through node v . Currently, the most commonly used method for computing the exact betweenness centrality (BC) is Brandes' algorithm [43]. For an unweighted

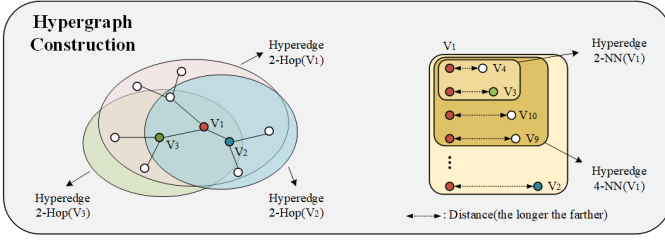


Fig. 2. The Principle of Hypergraph Generation by K-Hop and K-NN.

graph with n nodes and m edges, its time complexity is $\mathcal{O}(nm)$. This implies that for dense graphs, the complexity approaches $\mathcal{O}(n^2)$, making it computationally expensive. To address this issue, we propose training a GAT with a global receptive field as a predictor for betweenness centrality, denoted as BC_{GAT} . The computational complexity of this method is reduced to $\mathcal{O}(H_{ead}h_{hidden}^2m)$, where H_{ead} is the sum of the attention heads of all layers in the BC_{GAT} , h_{hidden} is the output dimension size at attention head, and m is the number of edges in the graph. Experimental results demonstrate that the BC values predicted by BC_{GAT} model are sufficiently accurate to allow the NCR-HoK framework to effectively perform network robustness curve prediction tasks. The loss of BC_{GAT} training can be expressed as follows:

$$Loss_{BC_{GAT}} = MSE(BC_{GAT}(v_i) - BC_{True}(v_i)) \quad (6)$$

where $BC_{GAT}(v_i)$ denotes the BC of node v_i predicted by the GAT [44] and $BC_{True}(v_i)$ denotes the ground true BC of node v_i .

Specifically, for each node v_i , the initial features $F(v_i)$ can be defined as follows:

$$F(v_i) = Linear(X_{v_i}^{out-deg} || X_{v_i}^{in-deg} || BC_{GAT}(v_i)) \quad (7)$$

where $X_{v_i}^{out-deg}$, $X_{v_i}^{in-deg}$ and $BC_{GAT}(v_i)$ represent the node's in-degree, out-degree, and betweenness centrality inferred by the BC_{GAT} with frozen parameters, respectively. Notably, these three embedding vectors are learned through three independent encoders. Besides, $||$ represent the concatenation operation.

B. Network High-Order Relation Generator

The core strength of our model NCR-HoK lies in its ability to uncover the latent relationships between high-order knowledge of graphs and network controllability robustness. This is achieved through the integration of hypergraph attention neural networks, where the generation of hypergraphs plays a crucial role. As shown in Fig.2, we utilized the K-Hop method to generate the initial structure of the hypergraph. Specifically, this method considers any set of nodes in a graph, where the distance between any two nodes does not exceed K hops, as a hyperedge, forming a hypergraph $HG_{K-Hop}(g)$ where g denotes the network index. This approach allows NCR-HoK to capture high-order connectivity patterns within local neighborhoods, thereby gaining a deeper understanding of the intrinsic characteristics of graph structures. The construction of K-Hop hypergraphs helps reveal how nodes in a graph

influence each other within a limited number of steps, providing a new perspective for understanding the dynamic changes and controllable robustness of graphs.

Moreover, we utilize the K-NN method to generate a more complex hypergraph structure. By calculating the distances between the embedding representations of nodes within the hypergraph embedding space, we connect each node to its K nearest neighbors to form hyperedges, generating hypergraph $HG_{K-NN}(g)$, where g denotes the network index. This approach not only considers the direct connectivity between nodes but also their similarity in the embedding space, thereby capturing more covert structures and features within the graph. The hypergraphs generated through the K-NN method enable NCR-HoK to adaptively explore and learn the graph's hidden and high-order features, providing robust support for predicting the graph's controllable robustness curve.

C. Graph Attention Neural Network Module

In order to learn underlying graph structures and improve the prediction of controllable robustness curves of graphs, we employ a dual-channel embedding approach combining GAT Neural Network Module and Dual HGNN Neural Network Module. The GAT Neural Network Module is particularly inclined towards learning explicit structural features present in the original graph.

Let $h^l(v_i)$ represent the embedding features of node v_i at layer l , where $h^0(v_i) = F(v_i)$. Input the adjacency matrix and encoded node features of the network into the Graph Attention Neural Network, where the feature transfer and aggregation between nodes can be represented as:

$$h^l(v_i) = \Phi\left(\sum_{e_{ij} \neq 0} \alpha_{ij} h^{l-1}(v_j)\right) \quad (8)$$

where Φ refers to a nonlinear layer and ReLU is used as activation function in our method. α_{ij} represents the attention coefficient between node v_i and its connected nodes v_j , which can be calculated using the following formula:

$$\alpha_{ij} = \frac{\exp(a_i^T \cdot u_j)}{\sum_{e_{ip} \neq 0} \exp(a_i^T \cdot u_p)} \quad (9)$$

$$u = ReLU(W \cdot h^{l-1}(v_i) + b) \quad (10)$$

where a_i^T is a trainable context vector, W and b are the transformation weights and biases of nodes in the trainable attention-ready state.

The above describes the working process of a single layer GAT Network. A GAT Neural Network Module consists of two layers of GAT Network. For each graph G_g , we concatenate its nodes to form the output of the GAT Network Module, serving as the graph embedding results for the graph.

D. Dual Hypergraph Attention Neural Network Module

By integrating the Dual HGNN Network, NCR-HoK not only focuses on the relationship between individual node and their neighbors, but also pays attention to complex interactions across multiple nodes, thereby providing richer and more in-depth feature representations. For the generated

hypergraphs $HG_{K-Hop}(g)$ and $HG_{K-NN}(g)$, we introduced a dual attention message passing module to learn the implicit and high-order features within these hypergraphs. Below, we describe the learning process of a single-layer hypergraph attention architecture for a hypergraph $HG_{K-Hop}(g)$.

1) *Node Attention on Hyperedge*: First, we use an attention-based message passing scheme to aggregate node information on hyperedges, thereby obtaining the embedding vectors of the hyperedge $h_{E-KHop}^l(e_j)$ generated in the hypergraph. Embedded representations of nodes in the l -th layer of the network can be regarded as $h_{N-KHop}^l(v_i)$, where $h_{N-KHop}^0(v_i) = F(v_i)$. For hyperedge e_j in hypergraph $HG_{K-Hop}(g)$, the learned feature of the layer can be described as:

$$h_{E-KHop}^l(e_j) = \Phi\left(\sum_{v_i \in e_j} \alpha_E(e_j, v_i) \cdot h_{N-KHop}^{l-1}(v_i)\right) \quad (11)$$

where $\alpha_E(e_j, v_i)$ is the attention coefficient of each node v_i on the hyperedge e_j , which can be calculated by the following formula:

$$\alpha_E(e_j, v_i) = \frac{\exp(a_2^T \cdot s_N(e_j, v_i))}{\sum_{v_{i'} \in e_j} (a_2^T \cdot s_N(e_j, v_{i'}))} \quad (12)$$

$$s_N(e_j, v_i) = ReLU(W_N \cdot h_{N-KHop}^{l-1}(v_i) + b_N) \quad (13)$$

where a_2^T is the trainable context vector, W_N and b_N are the transformation weights and biases with respect to the attention-ready state of the node, respectively.

2) *Hyperedge Attention on Node*: In the hypergraph, to update the embedding of node v_i at layer l , we use the following attention mechanism to aggregate information through hyperedges e_j connected to node v_i , which can be expressed as:

$$h_{N-KHop}^l(v_i) = \Phi\left(\sum_{e_j \supset v_i} \alpha_N(e_j, v_i) \cdot h_{E-KHop}^{l-1}(e_j)\right) \quad (14)$$

where $\alpha_N(e_j, v_i)$ is the attention coefficient about each hyperedge e_j passing through the node v_i , which can be calculated by the following formula:

$$\alpha_N(e_j, v_i) = \frac{\exp(a_3^T \cdot s_E(e_j, v_i))}{\sum_{e_{j'} \supset v_i} (a_3^T \cdot s_E(e_{j'}, v_i))} \quad (15)$$

$$s_E(e_j, v_i) = ReLU(W_E \cdot h_{E-KHop}^{l-1}(e_j) + b_E) \quad (16)$$

where a_3^T is the trainable context vector, W_E and b_E are the transformation weights and biases with respect to the attention-ready state of the node, respectively.

The process described above involves using a single-layer Dual HGNN Network for learning the embedding of hypergraph $HG_{K-Hop}(g)$. The Dual HGNN Neural Network Module includes two layers of Dual HGNN Network. We concatenate all the embedded nodes $h_{N-KHop}^l(v)$ in the hypergraph to serve as the output of the Dual HGNN Neural Network Module, which is used as the graph embedding results of the hypergraph $HG_{K-Hop}(g)$.

3) *The Dual Hypergraph Attention Neural Network Module on $HG_{K-NN}(g)$* : Similarly, for the hypergraphs $HG_{K-NN}(g)$ generated in the embedding space, we also use a Dual HGNN Neural Network Module to embed them. The feature of nodes in hypergraph $HG_{K-NN}(g)$ is represented by $h_{N-KNN}^l(v)$, where $h_{N-KNN}^0(v) = h_{N-KHop}^l(v)$.

E. Prediction of Network Controllable Robustness Curve

By using the GAT Neural Network Module and Dual HGNN Neural Network Module to learn embeddings from the original graph structure and hypergraphs HG_{K-Hop} and HG_{K-NN} , our model is supposed to capture explicit structural information in the original graph, high-order connectivity within local neighborhoods, and more hidden features in the embedding space. Before predicting controllable robustness curves using the input MLP module, the embedding features of the original graph $G(g)$ are formed by concatenating the features of each node from the three parts of embeddings mentioned above.

$$G(g)_{v_i} = h^l(v) \| h_{N-KHop}^l(v_i) \| h_{N-KNN}^l(v) \quad (17)$$

Then, using the MLP module and transforming the original graph $G(g)$ features into the final network controllable robustness curve, denoted as $PC(G(g))$, we get the controlled robustness curve prediction results made by NCR-HoK for the network $G(g)$.

Furthermore, we employ the SmoothL1Loss function to optimize our model, formulated as:

$$loss(x, y) = \frac{1}{N} \sum_{i=1}^N \begin{cases} 0.5 \cdot (PC_i - TC_i)^2, & \text{if } |PC_i - TC_i| < 1 \\ |PC_i - TC_i| - 0.5, & \text{otherwise} \end{cases} \quad (18)$$

where N is the number of nodes of the network, $PC \in R^{(N-1) \times 1}$ is the controlled robustness profile of the network obtained from the model prediction, and $TC \in R^{(N-1) \times 1}$ is the true controlled robustness profile of the network.

V. EXPERIMENTAL STUDIES

In this section, we evaluate the effectiveness and superiority of NCR-HoK through extensive experimental assessments. Initially, we introduce the datasets used in the experiments and the relevant parameter settings for our method as well as baseline methods. Subsequently, NCR-HoK is employed to predict the controlled robustness curves across various types of networks and corresponding experimental analyses are provided. Besides, ablation studies and parameter analysis are conducted to explore potential factors or modules that might influence the performance of NCR-HoK, shedding light on the potential improvement and application of our method.

A. Experimental Settings

1) *Datasets*: We evaluate the performance of proposed NCR-HoK on four typical directed and unweighted synthetic network models, including the Erdős-Rényi (ER) [45], generic scale-free (SF) [22], [46], [47], q-snapback [46], Newman-Watts small-world(NW) [24], Barabási-Albert (BA) scale-free networks [48].

Specifically, the edges in the ER network are added completely at random, where the direction of each edge is evenly randomly assigned. The edges of the SF network are generated according to their weights defined by:

$$w_i = (i + \theta)^{-\beta}, i = 1, 2, \dots, N \quad (19)$$

where $\beta \in [0, 1)$ and $\theta \ll N$. Two nodes v_j and v_i ($i \neq j, i, j = 1, 2, \dots, N$) are randomly picked with a probability

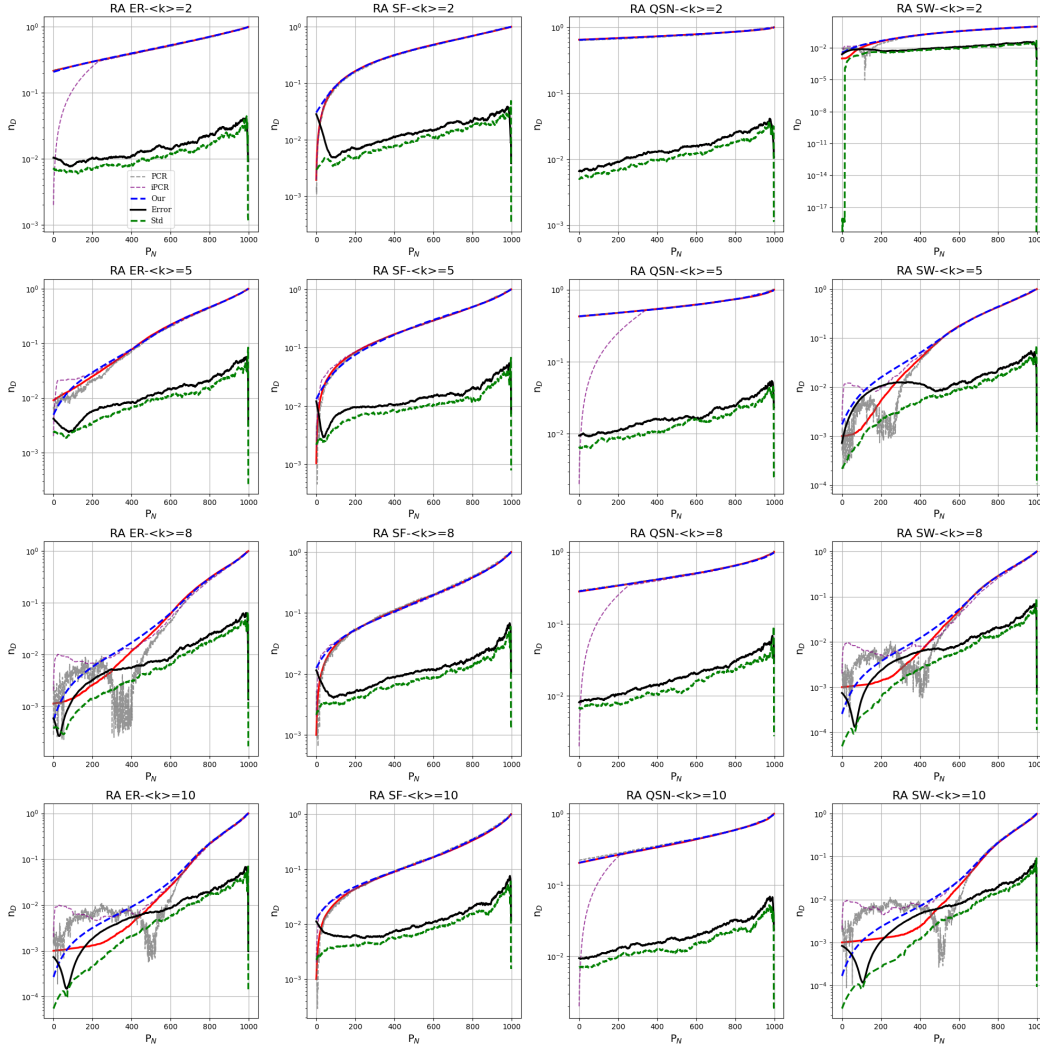


Fig. 3. The predictions of the controllable robustness curves for different network types under the RAs condition by NCR-HoK, PCR, and iPCR models. P_N represents the number of nodes having been removed from the network; and n_D is calculated by 1. RA (x)-< k >=(y) represents the true values of the controllable robustness curve under the RA condition for a network of type (x) with an average degree of (y), as well as the prediction results of each model.

proportional to the weights w_i and w_j , respectively. Then, an edge e_{ij} from i to j is added (if the two nodes are already connected, do nothing). The resulting SF network has a power-law distribution $k^{-\gamma}$, where k is the degree variable, with constant $\gamma = 1 + (1/\beta)$, which is independent of θ . In this article, β is set to 0.999 such that the power-law distribution has a reasonable scaling exponent $\gamma = 2.001$. The QSN has one layer r_q generated with a backbone chain and multiple snapback edges created for each node $i = r_q + 1, r_q + 2, \dots, N$, which connects backward to the previously appeared nodes $i - l \times r_q$ ($l = 1, 2, \dots, \lfloor i/r_q \rfloor$), with the same probability $q \in [0, 1]$. The SW network is initiated by a directed ring with $K = 2$ nearest-neighbors connected; that is, node v_i is connected to nodes v_{i-1} , v_{i-2} and v_{i+2} via edges $e_{i-1,i}$, $e_{i,i+1}$, $e_{i-2,i}$ and $e_{i,i+2}$. Then, adding or removing edges, until the predefined number of edges is reached.

Based on the adjacency matrix of each network topology, the initial hypergraph structure can be generated using the K-Hop method, with the corresponding adjacency matrix represented

as follows:

$$A_{ij} = \begin{cases} 0, & \text{if } v_i \notin e_j \\ 1, & \text{if } v_i \in e_j \end{cases} \quad (20)$$

Considering the limited length of the paper, after considering the simulation methodology of Randomized Attacks (RA), other types of attacks such as Target Degree Based Attacks (TDA) as well as Target Betweenness Based Attacks (TBA) can be investigated in the same manner, detailed results are presented in **Supplementary Materials VII. F**. All experiments are carried out on a computer with a 64-bit operating system, installed with two Intel i7-11700K (3.6GHz) and four NVIDIA Geforce RTX 3090. Baseline models are implemented using the default settings described in their original papers.

2) *Reproducibility*: During the training process, the epoch is set to 10 based on experience, and the structure that performed best on the validation data is chosen as the optimal model structure. We use the Adam optimizer to optimize formula 18, with a decay rate of 0.5, a learning rate of 0.001, an l_2 regularization coefficient of $1e-6$, and a gradient clipping value

TABLE I

THE AVERAGE ERRORS $\overline{e\tau}$ AND AVERAGE STANDARD DEVIATIONS $\overline{\sigma}$ OF THE CONTROLLABLE ROBUSTNESS CURVE PREDICTING FOR VARIOUS TYPES OF NETWORKS UNDER THE RA CONDITION ARE COMPARED AMONG THE NCR-HoK, PCR [27], iPCR [28] MODELS AND CRL-SGNN [29], ALONG WITH A COMPREHENSIVE RANKING.

			$\langle k \rangle = 2$	$\langle k \rangle = 5$	$\langle k \rangle = 8$	$\langle k \rangle = 10$	Average
ER	PCR	$\overline{e\tau}$	0.020	0.016	0.014	0.014	0.016(#2)
		$\overline{\sigma}$	0.015	0.019	0.020	0.022	0.019(#2)
	iPCR	$\overline{e\tau}$	0.043	0.015	0.017	0.013	0.022(#3)
		$\overline{\sigma}$	0.054	0.018	0.022	0.020	0.029(#4)
	CRL-SGNN	$\overline{e\tau}$	0.029	0.034	0.020	0.014	0.024(#4)
		$\overline{\sigma}$	0.016	0.043	0.021	0.022	0.026(#3)
	Our	$\overline{e\tau}$	0.016	0.015	0.012	0.010	0.013(#1)
		$\overline{\sigma}$	0.012	0.011	0.009	0.008	0.010(#1)
SF	PCR	$\overline{e\tau}$	0.017	0.020	0.021	0.024	0.021(#2)
		$\overline{\sigma}$	0.014	0.018	0.020	0.022	0.019(#2)
	iPCR	$\overline{e\tau}$	0.017	0.100	0.061	0.042	0.055(#4)
		$\overline{\sigma}$	0.015	0.012	0.073	0.050	0.038(#4)
	CRL-SGNN	$\overline{e\tau}$	0.023	0.027	0.022	0.014	0.022(#3)
		$\overline{\sigma}$	0.028	0.034	0.018	0.020	0.025(#3)
	Our	$\overline{e\tau}$	0.016	0.019	0.021	0.021	0.019(#1)
		$\overline{\sigma}$	0.012	0.015	0.015	0.016	0.015(#1)
QSN	PCR	$\overline{e\tau}$	0.015	0.016	0.012	0.011	0.014(#2)
		$\overline{\sigma}$	0.015	0.016	0.016	0.017	0.016(#2)
	iPCR	$\overline{e\tau}$	0.015	0.013	0.013	0.011	0.013(#1)
		$\overline{\sigma}$	0.015	0.016	0.016	0.016	0.016(#2)
	CRL-SGNN	$\overline{e\tau}$	0.024	0.043	0.023	0.045	0.034(#4)
		$\overline{\sigma}$	0.025	0.050	0.029	0.047	0.038(#4)
	Our	$\overline{e\tau}$	0.015	0.015	0.013	0.012	0.014(#2)
		$\overline{\sigma}$	0.011	0.011	0.009	0.008	0.010(#1)
SW	PCR	$\overline{e\tau}$	0.013	0.014	0.014	0.014	0.014(#2)
		$\overline{\sigma}$	0.014	0.018	0.021	0.023	0.019(#2)
	iPCR	$\overline{e\tau}$	0.014	0.014	0.017	0.012	0.014(#2)
		$\overline{\sigma}$	0.014	0.016	0.022	0.017	0.017(#2)
	CRL-SGNN	$\overline{e\tau}$	0.029	0.040	0.039	0.030	0.035(#4)
		$\overline{\sigma}$	0.032	0.042	0.044	0.032	0.038(#4)
	Our	$\overline{e\tau}$	0.012	0.014	0.012	0.010	0.012(#1)
		$\overline{\sigma}$	0.009	0.009	0.008	0.007	0.008(#1)

of 0.8. Additionally, the hypergraph generation part utilizes both the 3-Hop and 10-NN methods to generate the corresponding hypergraph structures. The selected K values (3-Hop and 10-NN) strike a good balance between capturing comprehensive higher-order knowledge and maintaining computational efficiency. Detailed analysis can be found in **Supplementary Materials VII. E**. During the pretraining of BC_{GAT} , we generated 4000 training samples for each of the four graph types: ER, SF, QSN and SW. For each graph, the number of nodes was randomly selected from the range [800, 1600], and the average node degree $\langle k \rangle$ was randomly chosen from 2, 5, 8, and 10. The detailed architecture of the BC_{GAT} model is provided in table S1.

B. Network Controllability Robustness Learning

1) *Controllability Robustness Curve Prediction*: In this section, we demonstrate the prediction of controllable robustness curves under RA conditions for NCR-HoK across different network topologies. Specifically, we address four types of network topologies: ER, SF, QSN, and SW. For each topology, we randomly generate 800 networks with average out-degrees of $\langle k \rangle = 2, 5, 8, 10$, resulting in a variety of network styles and a total of 12800 network datasets. These datasets are shuffled to serve as training samples for NCR-HoK. Additionally, for each type of network topology, each individually generates 100 network data as a test sample,

TABLE II

THE AVERAGE ERRORS AND STANDARD DEVIATIONS OF THE CONTROLLABLE ROBUSTNESS CURVE PREDICTING FOR VARIOUS TYPES OF NETWORKS WITH DIFFERENT AVERAGE DEGREES UNDER THE RA CONDITION ARE COMPARED AMONG THE NCR-HoK, PCR [27], iPCR [28] AND CRL-SGNN [29] MODELS, ALONG WITH A COMPREHENSIVE RANKING.

			ER	SF	QSN	SW	Average
$\langle k \rangle = 4$	PCR	$\overline{e\tau}$	0.019	0.030	0.018	0.021	0.022(#2)
		$\overline{\sigma}$	0.017	0.018	0.016	0.018	0.017(#2)
	iPCR	$\overline{e\tau}$	0.030	0.109	0.029	0.030	0.050(#4)
		$\overline{\sigma}$	0.021	0.140	0.018	0.024	0.051(#4)
	CRL-SGNN	$\overline{e\tau}$	0.052	0.044	0.035	0.035	0.042(#3)
		$\overline{\sigma}$	0.057	0.045	0.040	0.041	0.028(#3)
	Our	$\overline{e\tau}$	0.016	0.020	0.017	0.022	0.019(#1)
		$\overline{\sigma}$	0.012	0.015	0.012	0.012	0.013(#1)
$\langle k \rangle = 7$	PCR	$\overline{e\tau}$	0.013	0.024	0.016	0.013	0.017(#2)
		$\overline{\sigma}$	0.018	0.020	0.021	0.020	0.020(#2)
	iPCR	$\overline{e\tau}$	0.023	0.073	0.018	0.018	0.033(#4)
		$\overline{\sigma}$	0.024	0.087	0.018	0.022	0.038(#4)
	CRL-SGNN	$\overline{e\tau}$	0.039	0.030	0.023	0.026	0.030(#3)
		$\overline{\sigma}$	0.025	0.030	0.026	0.030	0.028(#3)
	Our	$\overline{e\tau}$	0.013	0.022	0.014	0.014	0.016(#1)
		$\overline{\sigma}$	0.009	0.016	0.010	0.009	0.011(#1)

totaling 1600 networks. The results obtained can be seen in Fig.3 and table I

Fig.3 displays the predicted results of the controllable robustness curves for different network topologies under RA conditions by NCR-HoK. Networks with the same average degree are aligned in a row, and each column represents the

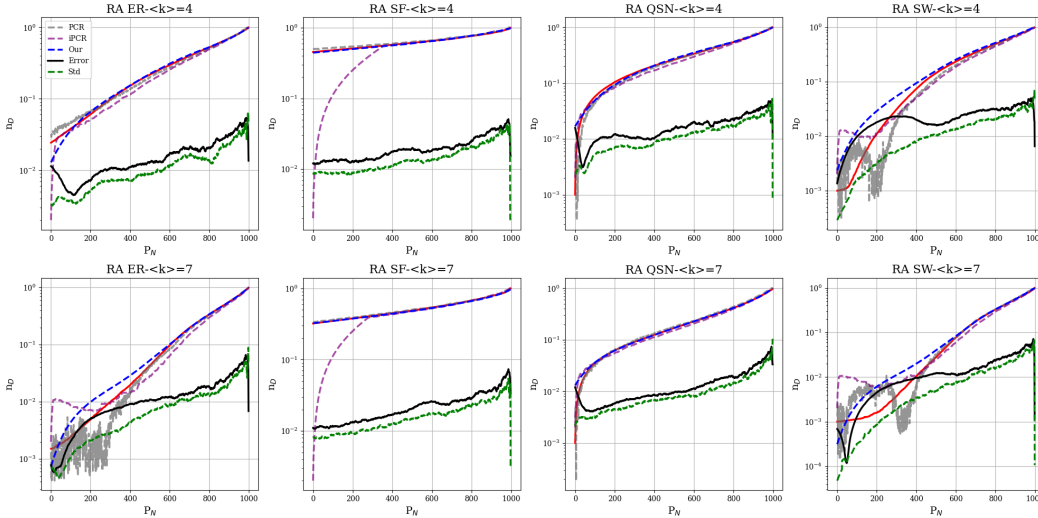


Fig. 4. The predictions of the controllable robustness curves for different types of network under the RA condition by NCR-HoK, PCR [27], iPCR [28] and CRL-SGNN [29] models. P_N represents the number of nodes having been removed from the network; and n_D is calculated by 1. RA $(x) - \langle k \rangle = (y)$ represents the true values of the controllable robustness curve under the RA condition for a network of type (x) with an average degree of (y) , as well as the prediction results of each model.

same network topology, with average degrees increasing from top to bottom. The red curve represents the average controllable robustness curve obtained through attack simulations. The blue curve (Our) shows the average controllable robustness curve predicted by NCR-HoK for different network topologies. The black curve (Error) indicates the error between predicted and actual values. The blue curve (Std) represents the standard deviation between predicted and actual values. The gray curve (PCR) shows the average controllable robustness curve predicted by the PCR model for different network topologies, and the purple curve (iPCR) represents the average controllable robustness curve predicted by the iPCR model for different network topologies.

It can be seen from Fig.3 that different network topologies exhibit varying trends in controllability robustness curves, and the effectiveness of different models in predicting these curves also varies. Specifically, NCR-HoK accurately predicts the controllability robustness curves for SF and QSN type networks, as evidenced by the blue prediction curve nearly perfectly aligning with the actual values. For ER and SW networks, NCR-HoK still performs well in predictions at lower average degrees. However, as the average degree increases, the predictive accuracy diminishes. This is due to the higher randomness in the topological connections of ER and SW networks, which lessens the impact of topological features on the network’s controllability robustness curves. Compared to the PCR and iPCR results, NCR-HoK’s predictions are smoother and more stable, as illustrated by the blue curve.

Table I shows the comparison results based on average errors \overline{eR} , standard deviations $\overline{\sigma}$, and overall rankings in the robustness learning of various types of networks under the condition of RA for NCR-HoK, PCR, iPCR and CRL-SGNN. We use “bleak bold” font to indicate the minimum prediction error value and the minimum prediction standard deviation value. It is shown from table I that aside from the QSN network, our

model’s prediction error and prediction standard deviation are the smallest on other graphs. This indicates that NCR-HoK’s network controllability robustness curve predictions are more precise and stable. Consequently, this leads to a more stable and smoother performance of the blue prediction curve in Fig.3. For the QSN network, we consider that its specific snapback structure may favor the ensemble CNN approach of iPCR.

TABLE III

THE AVERAGE ERRORS AND STANDARD DEVIATIONS OF THE CONTROLLABLE ROBUSTNESS CURVE PREDICTING FOR VARIOUS TYPES OF NETWORKS WITH DIFFERENT NODE SIZES UNDER THE RA CONDITION ARE COMPARED AMONG NCR-HoK, PCR [27], iPCR [28] AND CRL-SGNN [29] MODELS, ALONG WITH A COMPREHENSIVE RANKING.

		ER	SF	QSN	SW	Average	
N=800	PCR	\overline{eR}	0.012	0.026	0.013	0.011	0.016(#1)
		$\overline{\sigma}$	0.022	0.023	0.020	0.021	0.022(#2)
	iPCR	\overline{eR}	0.012	0.043	0.013	0.011	0.020(#2)
		$\overline{\sigma}$	0.022	0.044	0.019	0.021	0.027(#4)
CRL-SGNN	\overline{eR}	0.012	0.026	0.016	0.011	0.016(#1)	
	$\overline{\sigma}$	0.024	0.029	0.022	0.023	0.025(#3)	
Our	\overline{eR}	0.012	0.026	0.014	0.011	0.016(#1)	
	$\overline{\sigma}$	0.008	0.020	0.010	0.008	0.012(#1)	
N=1000	PCR	\overline{eR}	0.012	0.023	0.014	0.012	0.015(#2)
		$\overline{\sigma}$	0.018	0.021	0.017	0.019	0.019(#2)
	iPCR	\overline{eR}	0.012	0.050	0.014	0.012	0.022(#3)
		$\overline{\sigma}$	0.019	0.049	0.022	0.020	0.028(#4)
CRL-SGNN	\overline{eR}	0.016	0.036	0.021	0.017	0.023(#4)	
	$\overline{\sigma}$	0.023	0.027	0.026	0.024	0.025(#3)	
Our	\overline{eR}	0.011	0.023	0.013	0.010	0.014(#1)	
	$\overline{\sigma}$	0.008	0.017	0.009	0.008	0.011(#1)	
N=1200	PCR	\overline{eR}	0.011	0.026	0.018	0.011	0.017(#3)
		$\overline{\sigma}$	0.018	0.024	0.020	0.018	0.020(#2)
	iPCR	\overline{eR}	0.010	0.046	0.011	0.011	0.020(#2)
		$\overline{\sigma}$	0.016	0.053	0.017	0.018	0.026(#4)
CRL-SGNN	\overline{eR}	0.016	0.040	0.023	0.019	0.025(#4)	
	$\overline{\sigma}$	0.022	0.025	0.026	0.024	0.024(#3)	
Our	\overline{eR}	0.010	0.021	0.012	0.010	0.013(#1)	
	$\overline{\sigma}$	0.007	0.015	0.009	0.007	0.010(#1)	

2) Predicting the Controllability and Robustness Curves of Networks with Different Average Degrees: To explore

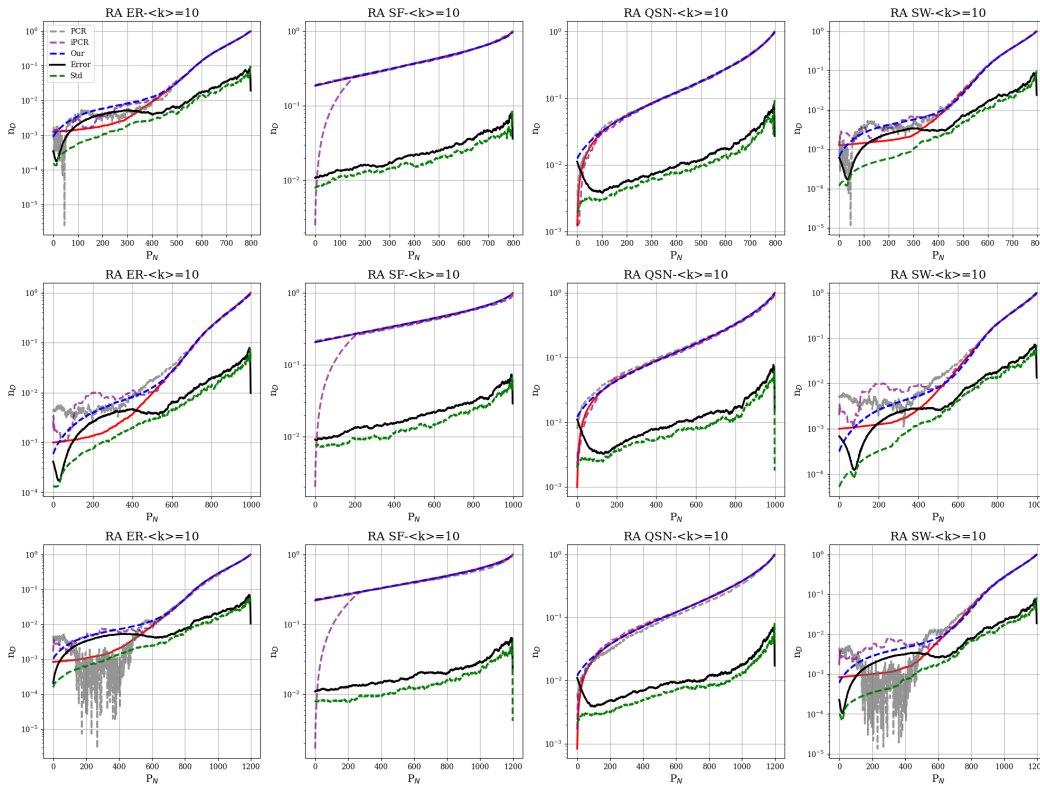


Fig. 5. The predictions of the controllable robustness curves for various types of network with different node sizes under the RAs condition by the NCR-HoK, PCR [27], iPCR [28] and CRL-SGNN [29] models.

TABLE IV
THE DETAILS OF REAL-WORLD NETWORKS USED IN THE EXPERIMENT.

Real-World Networks	Brief description	Node Number	Edge Number
DDG(DD-g97)	Protein	1021	5778
DEL(delaunay-n10)	DIMACS10 problem	1024	3056
DW5(dwt-1005)	Symmetric connection from Washington	1005	4813
DW7(dwt-1007)		1007	4791
LSH(lshp1009)	Alan George's L-shape problem	1009	3937
ORS(orsirr-1)	oil reservoir simulation	1030	6858

the transferability of NCR-HoK's learning on controllable robustness across networks with different average degrees, we conduct tests under the same RA conditions for four types of topological structures: ER, SF, QSN, and SW. We randomly generate 100 test samples for each network type with average out-degrees of $\langle k \rangle = 4$ and 7, respectively. The networks are tested using the NCR-HoK trained in Section V. A, and the results are shown in table II and Fig.4.

As can be seen from Fig.4, although NCR-HoK is trained on datasets with $\langle k \rangle = 2, 5, 8, 10$, it has good migration ability, and can still predict the controllable robustness curves of the network stably with $\langle k \rangle = 4, 7$. As shown by the blue line in the figure, the prediction curve is smoother and closer to the ground true relative to the baseline. On the other hand, the PCR and iPCR predictions are much steeper, especially the PCR, which shows a jittery behavior at the beginning. Combined with table II, it can be seen that the average error of NCR-HoK predictions is better than that of the baseline in most cases. In addition, the average standard deviation of NCR-HoK predictions is the smallest regardless of the network

topology, which indicates that NCR-HoK is able to maintain stable prediction results.

3) *Predicting the Controllability Robustness Curve of Networks with Different Node Sizes*: In order to explore the performance of NCR-HoK across networks of varying node sizes, we conduct experiments under the same RA conditions across four different topologies: ER, SF, QSN, and SW. We randomly generate 800 networks for each topology with an average out-degree of $\langle k \rangle = 10$ and different node scales. For each network topology, 100 individual networks are independently generated as test samples. We retrain NCR-HoK using datasets from different node sizes and complete the corresponding prediction tests. The results are shown in table III and Fig.5.

As can be seen from Fig.5, on SF and QSN networks, NCR-HoK is still able to give smooth and accurate predictions of network controllable robustness curves, while on ER and SW networks, NCR-HoK does not have good enough prediction performance in the early stage of the network controllable robustness, but it is still able to quickly approximate the trend

TABLE V
THE EVALUATION PERFORMANCE OF NCR-HoK, PCR [27], iPCR [28] AND CRL-SGNN [29] ON REAL-WORLD DATASETS.

Real-World Networks		DDG	DEL	DW5	DW7	LSH	ORS	Average
PCR	$\bar{e}\bar{r}$	0.053	0.210	0.157	0.146	0.195	0.147	0.151(#3)
	$\bar{\sigma}$	0.037	0.076	0.222	0.211	0.223	0.210	0.163(#3)
iPCR	$\bar{e}\bar{r}$	0.039	0.285	0.154	0.145	0.228	0.118	0.162(#4)
	$\bar{\sigma}$	0.023	0.116	0.221	0.214	0.223	0.193	0.165(#4)
CRL-SGNN	$\bar{e}\bar{r}$	0.033	0.043	0.119	0.091	0.123	0.205	0.102(#2)
	$\bar{\sigma}$	0.028	0.039	0.186	0.164	0.184	0.063	0.111(#2)
Our	$\bar{e}\bar{r}$	0.005	0.007	0.162	0.118	0.184	0.003	0.080(#1)
	$\bar{\sigma}$	0.013	0.017	0.012	0.015	0.011	0.008	0.013(#1)

of the network controllable robustness in the middle and late stages. And compared with the two baselines of PCR and iPCR, NCR-HoK is more stable. Combined with table III, for relatively small scale networks, PCR performs better than iPCR and CRL-SGNN. And the NCR-HoK prediction results are ranked first in terms of mean error and mean standard deviation.

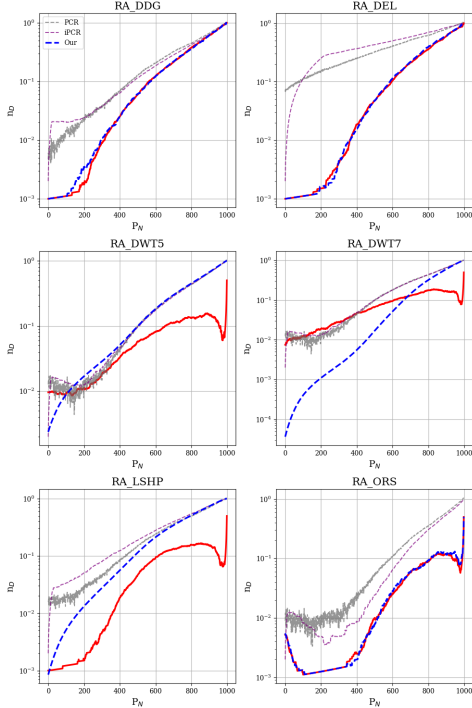


Fig. 6. Comparison of controllability robustness curve predicting results of NCR-HoK, PCR [27], iPCR [28] and CRL-SGNN [29] on real-world networks.

C. Robustness Learning for Real-World Networks

In addition to evaluating the performance of NCR-HoK on synthetic datasets, we also selected some real-world datasets from Network Repository¹ to assess the effectiveness and reliability of our model. The chosen datasets cover areas such as biological proteins, internet data, and oil industrial data, with detailed information presented in table IV. Since the node count in these datasets slightly exceeds 1000 nodes, following the method described in [28], we randomly select and remove some

nodes until the desired size was reached. For each network, we resize randomly 10 times and then averaged the prediction results and errors. The predicted results can be seen in table V and Fig.6.

TABLE VI
RESULTS OF ABLATION EXPERIMENTS WITH BC_{GAT} MODULE, *w.o. BC* INDICATES NO BC_{GAT} MODULE, *w.o. S-HGNN* INDICATES ONLY USING A SINGLE HGNN MODULE, *w.o. Dual HGNN* INDICATES NO DUAL HGNN MODULE, *Raw* INDICATES ORIGINAL SETTING.

			$\langle k \rangle = 2$	$\langle k \rangle = 5$	$\langle k \rangle = 8$	$\langle k \rangle = 10$
ER	<i>w.o. BC</i>	$\bar{e}\bar{r}$	0.037	0.027	0.017	0.017
		$\bar{\sigma}$	0.020	0.014	0.012	0.011
	<i>w.o. S-HGNN</i>	$\bar{e}\bar{r}$	0.214	0.098	0.061	0.047
		$\bar{\sigma}$	0.018	0.018	0.012	0.011
	<i>w.o. Dual HGNN</i>	$\bar{e}\bar{r}$	0.340	0.105	0.056	0.044
$\bar{\sigma}$		0.036	0.021	0.012	0.010	
<i>Raw</i>	$\bar{e}\bar{r}$	0.016	0.015	0.012	0.010	
	$\bar{\sigma}$	0.012	0.011	0.009	0.008	
SF	<i>w.o. BC</i>	$\bar{e}\bar{r}$	0.041	0.021	0.030	0.030
		$\bar{\sigma}$	0.020	0.017	0.020	0.021
	<i>w.o. S-HGNN</i>	$\bar{e}\bar{r}$	0.359	0.287	0.225	0.200
		$\bar{\sigma}$	0.020	0.024	0.024	0.027
	<i>w.o. Dual HGNN</i>	$\bar{e}\bar{r}$	0.449	0.407	0.258	0.220
$\bar{\sigma}$		0.020	0.035	0.035	0.033	
<i>o. BC</i>	$\bar{e}\bar{r}$	0.016	0.019	0.021	0.021	
	$\bar{\sigma}$	0.012	0.015	0.015	0.016	
QSN	<i>w.o. BC</i>	$\bar{e}\bar{r}$	0.049	0.017	0.021	0.029
		$\bar{\sigma}$	0.019	0.012	0.011	0.014
	<i>w.o. S-HGNN</i>	$\bar{e}\bar{r}$	0.185	0.125	0.100	0.090
		$\bar{\sigma}$	0.019	0.019	0.015	0.018
	<i>w.o. Dual HGNN</i>	$\bar{e}\bar{r}$	0.202	0.145	0.017	0.017
$\bar{\sigma}$		0.022	0.020	0.016	0.016	
<i>o. BC</i>	$\bar{e}\bar{r}$	0.015	0.015	0.013	0.012	
	$\bar{\sigma}$	0.011	0.011	0.009	0.008	
SW	<i>w.o. BC</i>	$\bar{e}\bar{r}$	0.013	0.030	0.016	0.016
		$\bar{\sigma}$	0.010	0.014	0.012	0.010
	<i>w.o. S-HGNN</i>	$\bar{e}\bar{r}$	0.139	0.082	0.053	0.042
		$\bar{\sigma}$	0.013	0.013	0.012	0.010
	<i>w.o. Dual HGNN</i>	$\bar{e}\bar{r}$	0.127	0.090	0.017	0.017
$\bar{\sigma}$		0.013	0.016	0.011	0.010	
<i>o. BC</i>	$\bar{e}\bar{r}$	0.012	0.014	0.012	0.010	
	$\bar{\sigma}$	0.009	0.009	0.008	0.007	

From table V and Fig.6, it can be seen that NCR-HoK is better than other baselines, both in terms of accuracy and stability of prediction. Especially, on DDG, DEL and ORS datasets, NCR-HoK is able to predict the trend of the network's controllable robustness in the presence of random attacks very accurately. This suggests that NCR-HoK is somewhat applicable to the analysis of controllable robustness for real-life networks. For real-world networks including DW5, DW7 and LSH, we think their unique structural properties might not be fully captured by our current hypergraph construction

¹<http://networkrepository.com/>

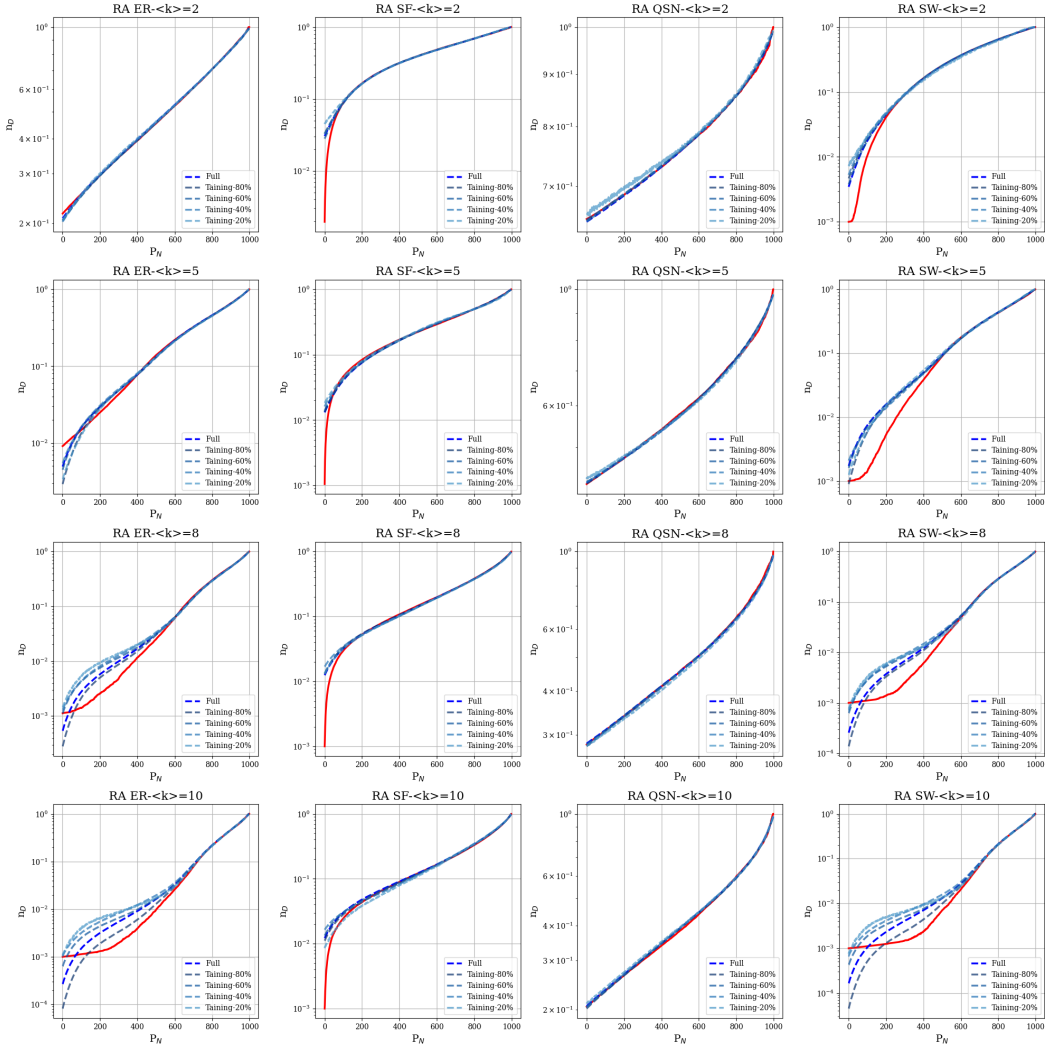


Fig. 7. NCR-HoK's controlled robustness curve prediction results for various networks under 20%, 40%, 60%, and 80% reduction of the training dataset, respectively.

methods and this is an area that needs to be improved in the future for our model.

D. Ablation Studies

To investigate the effectiveness of each component in our NCR-HoK model, we conduct a series of experiments. We evaluate the performance when removing the betweenness centrality feature (*w.o. BC*), removing both hypergraph attention channels (*w.o. Dual HGNN*), and using only a single hypergraph attention channel (*w.o. S-HGNN*). The performance of these variants of our method is compared against the full model (*Raw*). As shown in the table VI:

1) *Effectiveness of the BC_{GAT} module*: Across all datasets and thresholds, the models with the BC_{GAT} module (*o. BC*) consistently outperform the ones without it (*w.o. BC*), as indicated by the lower values of $\bar{e}\bar{r}$. This trend highlights the significant contribution of the BC_{GAT} component to capturing the critical structural features of the network that influence controllable robustness. Notably, for real-world networks like QSN and SW, the improvement is substantial, especially under

higher degree thresholds, demonstrating the model's scalability and robustness.

2) *Contribution of the Dual HGNN Architecture*: The experiments also underscore the importance of the hypergraph-based learning channels. When the entire Dual HGNN component is removed (*w.o. Dual HGNN*), leaving only the GAT module, the model's performance significantly deteriorates, demonstrating the necessity of hypergraph high-order information. Similarly, the *w.o. S-HGNN* experiment validates the importance of having two independent hypergraph channels by using only a single HGNN module. This variant exhibits a significant performance drop, highlighting the advantages of the dual-channel architecture.

E. Parameter Analysis

To assess the impact of data volume on model performance, as well as the contribution and effectiveness of key model components, we conduct parameter analysis experiments on the data samples used for model training and the k -values in hypergraph generation methods such as K-Hop and K-NN.

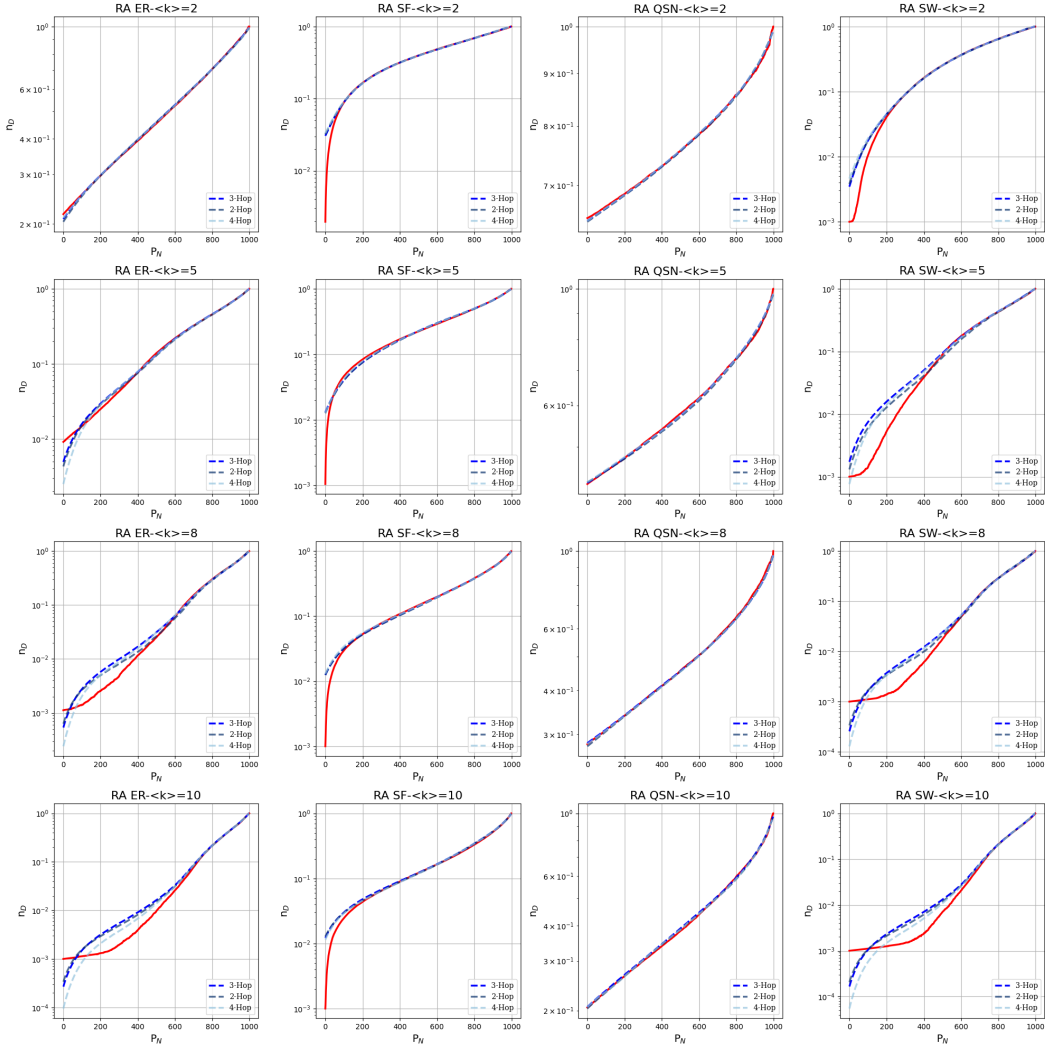


Fig. 8. The prediction results of NCR-HoK's controllable robustness curves for various network topologies for K-Hop's K-values of 2, 3, and 4 cases, respectively.

1) *Training Split*: According to the experimental setup in Section V. A, for each network topology with different average degrees $\langle k \rangle$, the original training sample consisted of 800 samples. In order to explore the impact of the amount of training data on model performance, the size of the training data is reduced to 20%, 40%, 60%, and 80% respectively, while the size of the test data samples remained unchanged. Some experimental results can be seen from **Supplementary Materials VII. D** due to page limitation.

Fig. 7 shows that for both types of network structures, SF and QSN, NCR-HoK is able to predict the controllable robustness curves of the network structures well for dataset sizes ranging from 20% to 100%. For the QSN network, when the dataset size is reduced to 20%, the prediction results of NCR-HoK (shown by the lightest blue line) show fluctuations, but the prediction curves are still generally in line with the trend of the controllable robustness curves. As for the ER and SW network structures, it can be seen that NCR-HoK is able to fit the network's controllable robustness curve well when the average network out-degree is low, but as the average network out-

degree increases, the pre-prediction effect of NCR-HoK on the network's controllable robustness curve gradually deteriorates. The best prediction is achieved with 80% training data volume while changing the size of the training dataset. And as can be seen from the results in table S2, the average error and standard deviation of NCR-HoK's predictions of controllable robustness profiles for a variety of network topologies remain at a low level for different training data sizes.

2) *The k-value of the K-Hop and K-NN*: In this section, in order to explore the impact of hypergraph structures constructed by K-Hop, K-NN methods on complex networks and embedding spaces on the performance of NCR-HoK, we analyze the ablation experiments by varying the K-value of the K-Hop and K-NN methods.

Similarly, following the experimental setup in Section V. A, we generate initial hypergraphs using the 2-Hop and 4-Hop. In the embedding space, we generate hypergraphs using the 5-NN, 20-NN, and 30-NN.

From Figs. 8 and 9, we can observe that NCR-HoK consistently gives better predictions of the controllable robustness

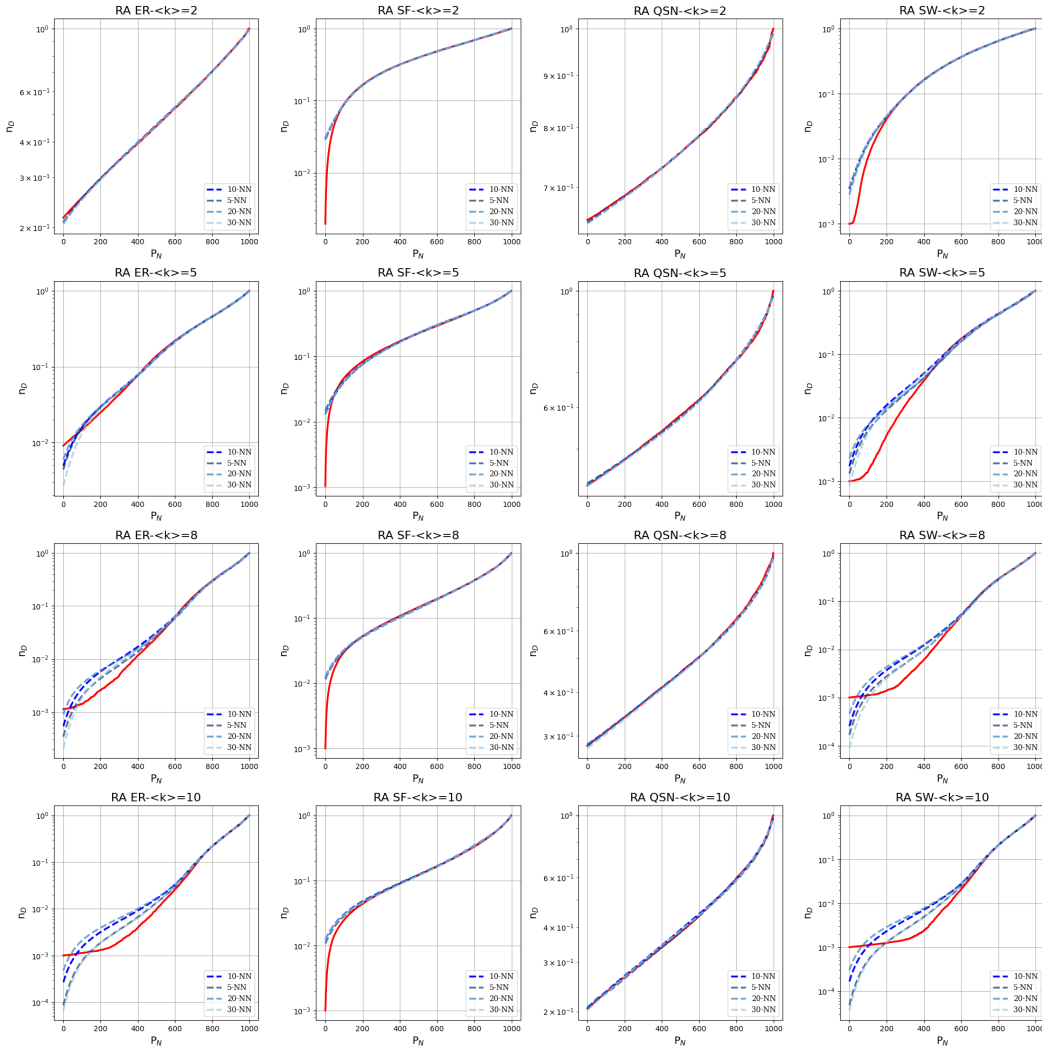


Fig. 9. The prediction results of NCR-HoK’s controllable robustness curves for various network topologies for K-NN’s K-values of 5, 10, 20 and 30 cases, respectively.

profiles of various networks under different K-value settings of the K-Hop and K-NN methods. When a larger value of K is chosen, such as 4-Hop or 30-NN, the predicted controllable robustness curves are closer to the true curves and more accurate. This may be due to the fact that the choice of K-value is equivalent to the feeling field of constructing the hypergraph, but when the K-value is larger, the constructed hypergraph covers more comprehensive high-order knowledge, so the prediction performance of the model will be better. The table of mean error and standard deviation results is detailed in the **Supplementary Materials Tables S3 and S4**.

F. Running Time Comparison

In addition to accuracy, another evaluation metric widely used to test the performance of network robustness learning algorithms is running time consumption. In this subsection, the time required to train the NCR-HoK model, the decreasing trend of training loss, and the time required to process a network with a node size of 1000 are discussed. All experiments, including baseline models, are conducted on the same computational

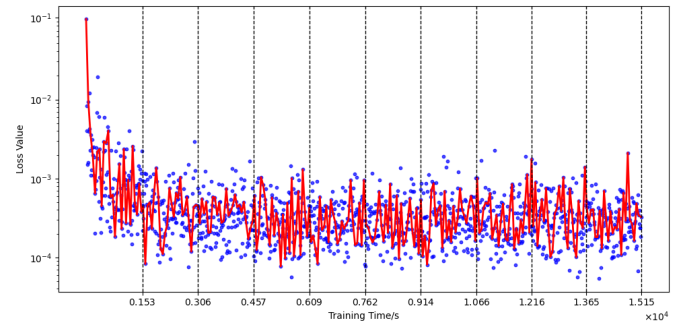


Fig. 10. The training process of NCR-HoK for 3200 networks with 1000 nodes.

platform to ensure fair and consistent comparisons. Baseline models are implemented using the default settings described in their original papers.

According to the experimental setup described in Section V. A, the average processing time per graph during model training is 0.118 seconds. In comparison, the PCR and iPCR

TABLE VII

THE AVERAGE TIME TAKEN TO PROCESS EACH GRAPH FOR RAS, PCR [27], iPCR [28], CRL-SGNN [29] AND NCR-HoK.

Controllability	Robustness	Unit: Second
RAS		23.581
PCR		0.306
iPCR		0.325
CRL-SGNN		0.029
NCR-HoK		0.085

models require 2.667 seconds and 5.898 seconds per graph, respectively, making NCR-HoK more efficient and simpler to train. As shown in Figure 10, training NCR-HoK for one epoch takes only 1530 seconds, and the loss decreases rapidly.

Table VII summarizes the average runtime across multiple independent tests using random attack simulations, PCR, iPCR, CRL-SGNN, and NCR-HoK on ER, SF, QSN, and SW networks, each with 1000 nodes and average degrees of $\langle k \rangle = 2, 5, 8, 10$. The results in the table indicate the average processing time per graph. It can be observed that, on graphs with 1000 nodes, compared to NCR-HoK (which is based on a spatial GNN framework), CRL-SGNN has a training and inference time of approximately 0.029 seconds per graph, which gives it a clear advantage due to its spectral GNN foundation. However, NCR-HoK still demonstrates significant advantages in terms of efficiency over the baseline methods including PCR and iPCR as well as traditional attack simulation approaches.

VI. CONCLUSION AND FEATURE WORK

This paper introduces NCR-HoK, a graph attention network that exploits high-order knowledge for robustness learning and controllability-robustness curve prediction. As the first systematic study of high-order hypergraph structures on controllable robustness, NCR-HoK integrates a node-feature encoder, hypergraphs built on high-order relations, and a dual-hypergraph attention module. The model simultaneously captures 1) explicit graph topology, 2) high-order neighborhood connections, and 3) latent structures in the embedding space—without expensive attack simulations. Experiments on synthetic and real-world networks demonstrate superior performance with low computational cost. Future work will extend controllability-robustness learning to broader classes of complex networks. However, to date, NCR-HoK cannot make predictions for time-varying, dynamic complex networks. This remains one of the existing research challenges. Therefore, future work will focus on developing controllability-based robustness learning and prediction methods for dynamic networks as well as more complex types of network such as attributed networks and heterogeneous networks.

REFERENCES

- [1] M. Newman, *Networks*. Oxford university press, 2018.
- [2] G. Chen and Y. Lou, "Naming Game," *Switzerland: Springer International Publishing*, 2019.
- [3] G. Chen, X. Wang, and X. Li, *Fundamentals of Complex Networks: Models, Structures and Dynamics*. John Wiley & Sons, 2014.
- [4] K. Börner, S. Sanyal, A. Vespignani *et al.*, "Network Science," *Annual Review of Information Science and Technology*, vol. 41, no. 1, pp. 537–607, 2007.
- [5] X. Teng, J. Liu, and M. Li, "Overlapping Community Detection in Directed and Undirected Attributed Networks Using a Multiobjective Evolutionary Algorithm," *IEEE Transactions on Cybernetics*, vol. 51, no. 1, pp. 138 – 150, 2021.
- [6] C. Gao, X. Teng, Y. Liu, and J. Liu, "A Bilevel-optimization-driven Evolutionary Algorithm for Community Detection in Multilayer Networks with Significant Topological Differences," *Chaos, Solitons & Fractals*, vol. 200, p. 116921, 2025.
- [7] Y.-Y. Liu, "Barab asi, A.-L., Control Principles of Complex Systems," *Reviews of Modern Physics, Rev Mod Phys*, vol. 88, p. 035006, 2016.
- [8] L. Xiang, F. Chen, W. Ren, and G. Chen, "Advances in Network Controllability," *IEEE Circuits and Systems Magazine*, vol. 19, no. 2, pp. 8–32, 2019.
- [9] Z. Yuan, C. Zhao, Z. Di, W.-X. Wang, and Y.-C. Lai, "Exact Controllability of Complex Networks," *Nature Communications*, vol. 4, no. 1, p. 2447, 2013.
- [10] Y.-Y. Liu, J.-J. Slotine, and A.-L. Barabási, "Controllability of Complex Networks," *Nature*, vol. 473, no. 7346, pp. 167–173, 2011.
- [11] L. Wang, X. Wang, and G. Chen, "Controllability of Networked Higher-Dimensional Systems with One-Dimensional Communication," *Philosophical Transactions of the Royal Society A: Mathematical, Physical and Engineering Sciences*, vol. 375, no. 2088, p. 20160215, 2017.
- [12] B. Hou, X. Li, and G. Chen, "The Roles of Input Matrix and Nodal Dynamics in Network Controllability," *IEEE Transactions on Control of Network Systems*, vol. 5, no. 4, pp. 1764–1774, 2017.
- [13] X. Teng, M. Zhong, and J. Liu, "A Self-Supervised Heterogeneous Graph Attention Model Based on Adaptable Step-Size Metapaths," *IEEE Transactions on Neural Networks and Learning Systems*, pp. 1–15, 2025.
- [14] J.-N. Wu, X. Li, and G. Chen, "Controllability of Deep-coupling Dynamical Networks," *IEEE Transactions on Circuits and Systems I: Regular Papers*, vol. 67, no. 12, pp. 5211–5222, 2020.
- [15] B. Hou, "Relevance of Network Characteristics to Controllability Degree," *IEEE Transactions on Automatic Control*, vol. 66, no. 11, pp. 5436–5443, 2020.
- [16] Y. Pan and X. Li, "Structural Controllability and Controlling Centrality of Temporal Networks," *PLoS One*, vol. 9, no. 4, p. e94998, 2014.
- [17] G. Menichetti, L. Dall'Asta, and G. Bianconi, "Network Controllability is Determined by the Density of Low In-degree and Out-degree nodes," *Physical Review Letters*, vol. 113, no. 7, p. 078701, 2014.
- [18] B. Hou, X. Li, and G. Chen, "Structural Controllability of Temporally Switching Networks," *IEEE Transactions on Circuits and Systems I: Regular Papers*, vol. 63, no. 10, pp. 1771–1781, 2016.
- [19] L. Wang, G. Chen, X. Wang, and W. K. Tang, "Controllability of Networked MIMO Systems," *Automatica*, vol. 69, pp. 405–409, 2016.
- [20] X. Tang, J. Liu, and M. Zhou, "Enhancing Network Robustness Against Targeted and Random Attacks Using a Memetic Algorithm," *Europhysics Letters*, vol. 111, no. 3, p. 38005, 2015.
- [21] J. C. Doyle, D. L. Alderson, L. Li, S. Low, M. Roughan, S. Shalunov, R. Tanaka, and W. Willinger, "The "Robust Yet Fragile" Nature of the Internet," *Proceedings of the National Academy of Sciences*, vol. 102, no. 41, pp. 14 497–14 502, 2005.
- [22] C.-L. Pu, W.-J. Pei, and A. Michaelson, "Robustness Analysis of Network Controllability," *Physica A: Statistical Mechanics and its Applications*, vol. 391, no. 18, pp. 4420–4425, 2012.
- [23] Y. Liu, J. Slotine, and A. Barabási, "Control Centrality and Hierarchical Structure in Complex Networks," *PLoS One*, vol. 7, no. 9, p. e44459, 2012.
- [24] Y. Lou, L. Wang, and G. Chen, "Toward Stronger Robustness of Network Controllability: A Snapback Network Model," *IEEE Transactions on Circuits and Systems I: Regular Papers*, vol. 65, no. 9, pp. 2983–2991, 2018.
- [25] G. Chen, Y. Lou, and L. Wang, "A Comparative Study on Controllability Robustness of Complex Networks," *IEEE Transactions on Circuits and Systems II: Express Briefs*, vol. 66, no. 5, pp. 828–832, 2019.
- [26] Y. Lou, L. Wang, and G. Chen, "Enhancing Controllability Robustness of Q-snapback Networks Through Redirecting Edges," *Research*, p. 7857534, 2019.
- [27] Y. Lou, Y. He, L. Wang, and G. Chen, "Predicting Network Controllability Robustness: A Convolutional Neural Network Approach," *IEEE Transactions on Cybernetics*, vol. 52, no. 5, pp. 4052–4063, 2020.
- [28] Y. Lou, Y. He, L. Wang, K. F. Tsang, and G. Chen, "Knowledge-Based Prediction of Network Controllability Robustness," *IEEE Transactions on Neural Networks and Learning Systems*, vol. 33, no. 10, pp. 5739–5750, 2021.

- [29] Y. Zhang, J. Ding, and X. Li, "Network controllability robustness learning via spatial graph neural networks," *IEEE Transactions on Network Science and Engineering*, vol. 11, no. 5, pp. 4045–4058, 2024.
- [30] X. Lu, Z. Liu, H. Xing, X. Xie, and C. Ye, "A Graph Convolutional Network Approach For Predicting Network Robustness," *Advances in Complex Systems*, vol. 27, no. 07n08, pp. 1–18, 2024.
- [31] Y. Feng, H. You, Z. Zhang, R. Ji, and Y. Gao, "Hypergraph Neural Networks," in *Proceedings of the AAAI conference on artificial intelligence*, vol. 33, no. 01, 2019, pp. 3558–3565.
- [32] Y. Gao, Y. Feng, S. Ji, and R. Ji, "HGNN+: General Hypergraph Neural Networks," *IEEE Transactions on Pattern Analysis and Machine Intelligence*, vol. 45, no. 3, pp. 3181–3199, 2022.
- [33] C. Chen, Z. Cheng, Z. Li, and M. Wang, "Hypergraph Attention Networks," in *2020 IEEE 19th International Conference on Trust, Security and Privacy in Computing and Communications*. IEEE, 2020, pp. 1560–1565.
- [34] Z. Mei, X. Bi, D. Li, W. Xia, F. Yang, and H. Wu, "DHHNN: a dynamic hypergraph hyperbolic neural network based on variational autoencoder for multimodal data integration and node classification," *Information Fusion*, vol. 119, p. 103016, 2025.
- [35] M.-R. Yang and X.-J. Xu, "Recent Advances in Hypergraph Neural Networks," *Journal of the Operations Research Society of China*, pp. 1–37, 2025.
- [36] Y. Gao, Z. Zhang, H. Lin, X. Zhao, S. Du, and C. Zou, "Hypergraph Learning: Methods and Practices," *IEEE Transactions on Pattern Analysis and Machine Intelligence*, vol. 44, no. 5, pp. 2548–2566, 2020.
- [37] A. Antelmi, G. Cordasco, M. Polato, V. Scarano, C. Spagnuolo, and D. Yang, "A Survey on Hypergraph Representation Learning," *ACM Computing Surveys*, vol. 56, no. 1, pp. 1–38, 2023.
- [38] S. Mo, X. Teng, K. Wu, J. Liu, and K. Yuan, "A Universal Subhypergraph-Assisted Embedding Framework for Both Homogeneous and Heterogeneous Networks," *IEEE Transactions on Knowledge and Data Engineering*, vol. 37, no. 9, pp. 4935–4947, 2025.
- [39] X. Zheng, Y. Luo, L. Sun, X. Ding, and J. Zhang, "A Novel Social Network Hybrid Recommender System Based on Hypergraph topologic structure," *World Wide Web*, vol. 21, pp. 985–1013, 2018.
- [40] K. Ding, J. Wang, J. Li, D. Li, and H. Liu, "Be more with less: Hypergraph attention networks for inductive text classification," in *Proceedings of the 2020 Conference on Empirical Methods in Natural Language Processing (EMNLP)*, 2020, pp. 4927–4936.
- [41] Y. Luo, "Shine: Subhypergraph Inductive Neural Network," *Advances in Neural Information Processing Systems*, vol. 35, pp. 18 779–18 792, 2022.
- [42] A. Mirhoseini, A. Goldie, M. Yazgan, J. W. Jiang, E. Songhori, S. Wang, Y.-J. Lee, E. Johnson, O. Pathak, A. Nazi *et al.*, "A Graph Placement Methodology for Fast Chip Design," *Nature*, vol. 594, no. 7862, pp. 207–212, 2021.
- [43] U. Brandes, "A Faster Algorithm for Betweenness Centrality," *Journal of Mathematical Sociology*, vol. 25, no. 2, pp. 163–177, 2001.
- [44] P. Veličković, G. Cucurull, A. Casanova, A. Romero, P. Liò, and Y. Bengio, "Graph Attention Networks," in *International Conference on Learning Representations*, 2018.
- [45] P. Erdős and A. Rényi, "On the Strength of Connectedness of a Random Graph," *Acta Mathematica Hungarica*, vol. 12, no. 1, pp. 261–267, 1961.
- [46] K.-I. Goh, B. Kahng, and D. Kim, "Universal Behavior of Load Distribution in Scale-Free Networks," *Physical Review Letters*, vol. 87, no. 27, p. 278701, 2001.
- [47] F. Sorrentino, "Effects of the Network Structural Properties on Its Controllability," *Chaos: An Interdisciplinary Journal of Nonlinear Science*, vol. 17, no. 3, 2007.
- [48] M. E. Newman and D. J. Watts, "Renormalization Group Analysis of the Small-World Network Model," *Physics Letters A*, vol. 263, no. 4–6, pp. 341–346, 1999.
- [49] K. Maile, E. Lecarpentier, H. Luga, and D. G. Wilson, "DARTS-PRIME: Regularization and scheduling improve constrained optimization in differentiable NAS," *arXiv preprint arXiv:2106.11655*, 2021.
- [50] H. Yue, P. Hong, and H. Liu, "Graph-Graph Similarity Network," *IEEE Transactions on Neural Networks and Learning Systems*, vol. 35, no. 7, pp. 9136–9146, 2022.
- [51] H. Wang, J. Yu, X. Wang, C. Chen, W. Zhang, and X. Lin, "Neural similarity search on supergraph containment," *IEEE Transactions on Knowledge and Data Engineering*, vol. 36, no. 1, pp. 281–295, 2023.
- [52] M. Isallari and I. Rekek, "Brain graph super-resolution using adversarial graph neural network with application to functional brain connectivity," *Medical Image Analysis*, vol. 71, p. 102084, 2021.
- [53] M. Lu, Z. Xiao, H. Li, Y. Zhang, and N. N. Xiong, "Feature pyramid-based graph convolutional neural network for graph classification," *Journal of Systems Architecture*, vol. 128, p. 102562, 2022.
- [54] X. Zhou and H. Wu, "scHiClassifier: a deep learning framework for cell type prediction by fusing multiple feature sets from single-cell Hi-C data," *Briefings in Bioinformatics*, vol. 26, no. 1, 2024.
- [55] X. Yang, K. K. Mann, H. Wu, and J. Ding, "scCross: a deep generative model for unifying single-cell multi-omics with seamless integration, cross-modal generation, and in silico exploration," *Genome Biology*, vol. 25, no. 1, p. 198, 2024.
- [56] S. Zhou, J. Zhang, W. Zuo, and C. C. Loy, "Cross-scale internal graph neural network for image super-resolution," *Advances in neural information processing systems*, vol. 33, pp. 3499–3509, 2020.
- [57] Z. Xia, W. Zhang, and Z. Weng, "Social Recommendation System Based on Hypergraph Attention Network," *Computational Intelligence and Neuroscience*, vol. 2021, no. 1, p. 7716214, 2021.
- [58] B. Yu, C. Xie, H. Cai, H. Duan, and P. Tang, "Meta-path and hypergraph fused distillation framework for heterogeneous information networks embedding," *Information Sciences*, vol. 667, p. 120453, 2024.
- [59] J. Zhu, A. Reganti, E. W. Huang, C. Dickens, N. Rao, K. Subbian, and D. Koutra, "Simplifying distributed neural network training on massive graphs: Randomized partitions improve model aggregation," *ACM Transactions on Knowledge Discovery from Data*, vol. 19, no. 1, pp. 1–26, 2025.
- [60] E. Chien, C. Pan, J. Peng, and O. Milenkovic, "You are AllSet: A Multiset Function Framework for Hypergraph Neural Networks," in *International Conference on Learning Representations*, 2020.
- [61] X. Zhi, "A Review of Hypergraph Neural Networks," *EAI Endorsed Transactions on e-Learning*, vol. 10, no. 1, 2024.
- [62] L. Bai, F. Hu, C. Tang, Z. Mei, and C. Liu, "Hyperbolic multi-channel hypergraph convolutional neural network based on multilayer hypergraph," *Scientific Reports*, vol. 15, no. 1, p. 24606, 2025.
- [63] S. Imai and A. Inokuchi, "Efficient supergraph search using graph coding," *IEICE TRANSACTIONS on Information and Systems*, vol. 103, no. 1, pp. 130–141, 2020.
- [64] Z. Chang, Y. Zhang, and H. C. Chen, "Neural Network Graph Similarity Computation Based on Graph Fusion," *arXiv preprint arXiv:2502.18291*, 2025.

Supplemental Materials for “High-order Knowledge Based Network Controllability Robustness Prediction: A Hypergraph Neural Network Approach”

Shibing Mo, Jiarui Zhang, Jiayu Xie, Xiangyi Teng, and Jing Liu

VII. SUPPLEMENTAL MATERIALS

A. Related Work

1) *The application of hypergraph neural networks*: Hypergraph neural networks — a term used in the literature with several related meanings (e.g., supernetworks that embed many candidate architectures, graph-of-graphs or hypergraph representations where each node is itself a graph, and extensions of hypergraph/hypergraph laplacians) — have already been applied across a remarkably broad set of domains and tasks. In neural architecture search, the differentiable search paradigm treats the search space as a single over-arching hypergraph (or supernetwork) that contains all candidate cells/paths and is optimized end-to-end, enabling efficient architecture optimization for image classification and related tasks [49]. In problems that compare or index whole graphs, researchers build a hypergraph of graphs (each node represents a data graph and edges encode pairwise similarities) so that graph-level classification, retrieval, or similarity search can be cast as node classification/lookup on the hypergraph; this idea underpins recent graph-graph similarity networks and neural hypergraph containment/search systems designed for large graph databases and efficient hypergraph queries [50], [51], [51]. In neuroscience and medical imaging, hypergraph and graph-super-resolution methods use graph neural models to upsample or refine low-resolution brain connectivity maps into higher-resolution connectomes, improving downstream analyses that require fine-grained regional networks [52]. Engineering applications have also adopted hypergraph-style architectures: spatial-temporal hypergraph feature extractors and multi-scale hypergraph convolutional modules have been proposed for rotating machinery fault diagnosis and structural health monitoring, where mapping multi-sensor signals into graphs and then into hypergraph representations yields robust features for anomaly detection [31], [53]. Additionally, the interactive concept of supergraph neural networks can be applied to integrate multi-modal and multi-feature scenarios in single-cell multi-omics [54], [55]. In image processing, graph-based and hypergraph-inspired GNNs support multi-image and cross-scale super-resolution / restoration tasks by modeling nonlocal self-similarities across patches as graph nodes and using graph message passing to aggregate complementary information from multiple observations [56]. Recommender systems and social recommendation have benefited from hypergraph and hypergraph constructions (often implemented via HGNN [31] variants) that explicitly model multi-party interactions, social groups, and multi-view modalities to better capture group influence and high-order affinities; empirical

studies report improved recommendation and robustness when hypergraph/hypergraph attention mechanisms are used [57], [58]. From a systems and scalability perspective, the hypergraph abstraction is useful for distributed or federated GNN training: constructing a hypergraph to summarize or index many local graphs (or to cluster nodes/partitions) can reduce communication and speed up training on massive graph collections [59]. Beyond these concrete applications, surveys and reviews of hypergraph and hypergraph methodologies highlight how hypergraph laplacians, hypergraph generalizations, and hypergraph kernels provide principled theoretical foundations that have catalyzed diverse applications in multimodal fusion, biological network analysis, document and text classification, and knowledge-graph style queries; these reviews also point to ongoing research on efficiency, attention-based weighting of hyperedges, and multiset / AllSet [60] style propagation rules that extend the expressive power of conventional GNNs [61], [62]. Finally, recent work on neural similarity search, graph coding for efficient hypergraph search, and specialized index structures shows that hypergraph neural methods are not only beneficial for predictive modeling but also for practical graph-database operations such as containment search and large-scale retrieval, making them attractive for industrial graph-mining, cheminformatics, and program analysis pipelines [51], [63], [64].

B. Formalizing High-order Knowledge

This subsection gives a concise formal definition of high-order knowledge, states two propositions that make precise why hypergraph-derived features are strictly richer than 1-hop (pairwise) features for many controllability/robustness targets, and explains how these results connect to the Dual HGNN formulas 11-16.

1) *Notation*: Let $G = (V, E)$ be a simple graph with $|V| = n$ nodes and adjacency matrix $A \in \{0, 1\}^{n \times n}$. For an integer $K \geq 1$ denote the set of walk matrices $\{A, A^2, \dots, A^K\}$. For a hypergraph constructed on V with m hyperedges, let $H \in \{0, 1\}^{n \times m}$ be its node-hyperedge incidence matrix and let $W \in \mathbb{R}^{m \times m}$ be a diagonal matrix of hyperedge weights. Define the node-projection matrix $B := HWH^T \in \mathbb{R}^{n \times n}$. When needed, we write entrywise relations as B_{ij} . We denote by \mathcal{A}_K the algebra generated by the matrices $\{I, A, A^2, \dots, A^K\}$ under linear combinations and (optional) elementwise boolean thresholding.

2) *High-order knowledge Definition*: A feature object (matrix/tensor/collection) \mathcal{H} computed from G is said to encode

high-order knowledge of order K if \mathcal{H} depends nontrivially on walk information of length up to K ; equivalently,

- \mathcal{H} lies in the algebra generated by $\{A, A^2, \dots, A^K\}$ but not in the subalgebra generated by $\{I, A\}$ alone, or
- \mathcal{H} is produced by a hypergraph incidence H whose construction uses K -ball / K -step relations (e.g., K -Hop hyperedges) or a kernel/diffusion $\Psi(A)$ incorporating powers up to degree K (e.g., embeddings derived from spectral/propagation maps).

Intuitively, high-order refers to information that cannot be recovered from only immediate-neighbor (1-hop) relations.

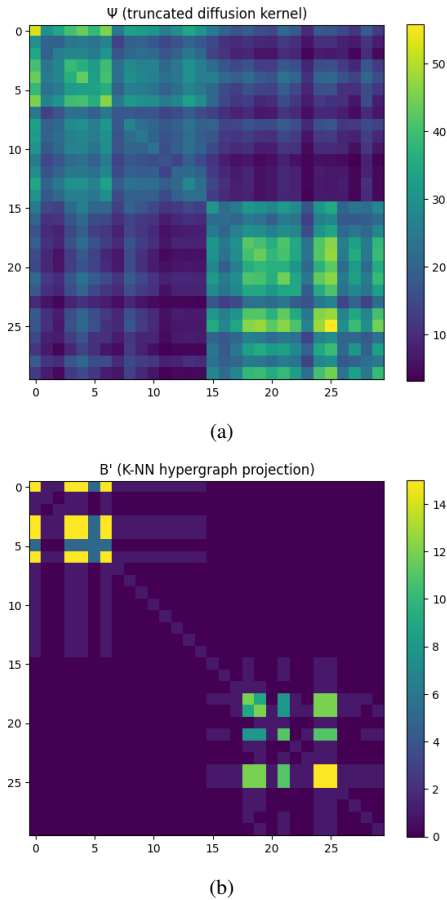


Fig. S1. Visualization results of the corresponding matrix to compare large entries of ψ and B' (with top pairs overlapping).

3) *Propositions*: We state two propositions that formalize the intuition that K -Hop and K -NN hypergraphs (as used in this work) encode strictly more information than 1-hop adjacency for many targets of interest.

i) *Proposition 1 (K-Hop hypergraph sufficiency)*. Let $HG_{K\text{-Hop}}$ be the hypergraph constructed by taking, for each node $v \in V$, the K -ball $\mathcal{N}_K(v) := \{u : \exists k \leq K, (A^k)_{uv} > 0\}$ as a hyperedge (or by using a collection of such balls), and let H be its incidence matrix. Then the node-projection matrix $B = HWH^T$ is a function of the family $\{A, A^2, \dots, A^K\}$. Consequently, under (Assum1) there exists a map \mathcal{F} (possibly nonlinear) such that $R(G) = g(\sum_{k=1}^K \alpha_k A^k) = g(\mathcal{F}(B))$. Hence any predictor that has access to B (or learnable

transforms of B) can in principle recover the dependence of $R(G)$ expressed in (Assum1).

Proof (sketch). For each center v define the indicator vector $\mathbf{1}_{\mathcal{N}_K(v)} \in \{0, 1\}^n$ where the i -th entry equals 1 iff there exists a walk of length $\leq K$ from v to i ; equivalently this indicator depends only on the booleanized sum $\mathbf{1}(\sum_{k=1}^K A^k > 0)$. If the hyperedge set contains the K -balls (one per center) and weights in W are chosen deterministically (e.g., all ones), then $B = \sum_{v \in V} \mathbf{1}_{\mathcal{N}_K(v)} \mathbf{1}_{\mathcal{N}_K(v)}^T$, which shows that each entry B_{ij} is a count of how many K -balls contain both i and j . Therefore every entry of B is a function of the booleanized matrices $\{(\mathbf{1}(A^k > 0))\}_{k \leq K}$ (and hence of $\{A^k\}_{k \leq K}$ up to thresholding). As the right-hand side in (Assum1) depends only on $\{A^k\}_{k \leq K}$, there exists a (possibly many-to-one) map \mathcal{F} from B to $\sum_{k \leq K} \alpha_k A^k$ (or to sufficient statistics for g). Thus the stated equality follows.

Remark. Exact algebraic invertibility (i.e., uniquely recovering A^k from B) is not required: it suffices that the information in B contains the sufficient statistics used by g . In practice, the Dual HGNN learns \mathcal{F} or an approximation thereof.

ii) *Proposition 2 (K-NN hypergraph and diffusion kernels)*. Let $\Phi : V \rightarrow \mathbb{R}^d$ be node embeddings such that the pairwise similarity matrix S with entries $S_{ij} = \langle \Phi(i), \Phi(j) \rangle$ approximates a diffusion kernel of the adjacency, $S \approx \Psi(A) := \sum_{k=0}^{\infty} \beta_k A^k$, with the truncation $\sum_{k=0}^K \beta_k A^k$ dominating contributions up to order K . Constructing a K -NN hypergraph by linking each node to its K_{NN} nearest neighbors in embedding space yields a projection matrix B' whose large entries correspond to large entries of $\Psi(A)$. If $R(G)$ depends on structural equivalence or diffusion-based proximity (i.e. on $\Psi(A)$), then B' is informative for predicting $R(G)$ while 1-hop adjacency alone is not.

Proof (sketch).

Under the approximation $S \approx \Psi(A)$ assume the approximation error is small in operator norm on the subspace of interest. Thresholding or taking the K -NN of S selects pairs with the largest values of $\Psi(A)_{ij}$, which reflect sums of weighted walk counts between nodes up to order K . The resulting incidence matrix H' and projection $B' = H'W'H'^T$ therefore encode (thresholded) diffusion information and role-similarity that go beyond immediate adjacency. If $R(G)$ depends on such diffusion or role-based features, a model using B' can access them while a model restricted to functions of A with degree ≤ 1 cannot, concluding the claim.

Besides, we provide some numerical analysis as follows:

Fig. S1 (a) ψ represents the node embedding ψ (spectral embedding) generated by extracting the eigenvector of the diffusion kernel with a truncation order of 40. The Fig. S1 (b) visualizes the projection matrix B' computed after constructing a hypergraph using K -NN.

The heatmap of ψ displays larger diffusion affinity entries within two communities (two blocks of the matrix). These high values result from the accumulation of paths spanning multiple steps. The heatmap of B' reveals the “co-occurrence” structure preserved after K -NN hypergraph projection: most node pairs frequently co-occurring within the same hyperedge manifest as large values in B' . The top-40 overlap rate ($\approx 45\%$) indicates that under this setting, the K -NN hypergraph indeed captures

TABLE S1
 BC_{GAT} MODEL NETWORK STRUCTURE

Layer Name	Layer Type	Input Channels	Output Channels	Number of Parameters
gat1	GATConv (4 heads)	1	64	$1 \times 64 \times 4 + 2 \times 64 \times 4 + 64 \times 4 = 1024$
gat2	GATConv (1 head)	$64 \times 4 = 256$	64	$256 \times 64 + 2 \times 64 + 64 = 16576$
fc	Fully Connected	64	1	$64 \times 1 + 1 = 65$

a portion of ψ 's major entries (particularly node pairs that are significantly close in the embedding space).

4) *Connection to Dual HGNN*: The Dual HGNN processes hypergraph structure via two alternating steps: node-to-hyperedge aggregation and hyperedge-to-node aggregation (formulas 11-16). These steps are learnable functions of the incidence matrix H and node/hyperedge features. Concretely, the message passing performed by the Dual HGNN can be written schematically as

$$X_E \leftarrow f_E(H^T, X), \quad X \leftarrow f_V(H, X_E),$$

where X and X_E are node and hyperedge feature matrices and each f includes attention weights that are learned (see formulas 11-16). Because the node-projection matrix $B = HWH^T$ is a sufficient statistic for the high-order relations described above (Propositions 1–2), the Dual HGNN has the representational capacity to learn maps of the form $X_{\text{out}} = \text{NN}(\mathcal{T}(B, X)) \approx \text{NN}(\mathcal{T}'(\{A^k\}_{k \leq K}, X))$, for suitable neural transforms $\mathcal{T}, \mathcal{T}'$ and a readout NN. In other words, by attending to hyperedges and aggregating across them the Dual HGNN implements learnable functions of high-order statistics (walk counts, diffusion affinities, and role-similarity) that are relevant to controllability/robustness targets and which are generally inaccessible to models restricted to 1-hop adjacency information.

In summary, under mild and natural assumptions on the dependence of the target on multi-step connectivity, K-Hop and K-NN hypergraphs provide a formal instantiation of high-order knowledge; the Dual HGNN is a principled mechanism to transform these high-order statistics into predictive node embeddings and graph-level summaries.

C. The Overview of BC_{GAT} Model Network Structure

Table S1 shows the network architecture of the BC_{GAT} model.

D. The Experimental Result of Training Split in Section V. D

The specific experimental results are shown in Table S2.

E. The Experimental Results of the Choice of K-value

1) *K-Hop Experiments on the different choice of K*: Based on the data in table S3, the choice of $K=3$ (3-Hop) appears to be a practical and well-balanced decision, representing an excellent trade-off between model performance and computational cost. As shown in the table results:

- **Marginal Performance Gains with Higher K** : When comparing the results of 3-Hop to 4-Hop, the performance improvements in terms of mean error and standard deviation are minimal to non-existent across all network types.

TABLE S2

THE MEAN ERROR $\bar{e}\bar{r}$ AND MEAN STANDARD DEVIATION $\bar{\sigma}$ OF THE CONTROLLED ROBUSTNESS CURVES OF NCR-HoK'S PREDICTION FOR DIFFERENT NETWORK TOPOLOGIES ARE REDUCED BY 20%, 40%, 60%, AND 80% FOR THE TRAINING DATASET, RESPECTIVELY.

RA Attack			$\langle k \rangle = 2$	$\langle k \rangle = 5$	$\langle k \rangle = 8$	$\langle k \rangle = 10$
20%	ER	$\bar{e}\bar{r}$	0.019	0.015	0.016	0.012
		$\bar{\sigma}$	0.014	0.011	0.010	0.008
	SF	$\bar{e}\bar{r}$	0.020	0.022	0.023	0.023
		$\bar{\sigma}$	0.016	0.016	0.017	0.017
	QSN	$\bar{e}\bar{r}$	0.016	0.018	0.016	0.016
		$\bar{\sigma}$	0.012	0.012	0.011	0.011
	SW	$\bar{e}\bar{r}$	0.016	0.015	0.014	0.011
		$\bar{\sigma}$	0.010	0.011	0.009	0.008
40%	ER	$\bar{e}\bar{r}$	0.017	0.015	0.014	0.012
		$\bar{\sigma}$	0.013	0.011	0.009	0.008
	SF	$\bar{e}\bar{r}$	0.016	0.019	0.020	0.022
		$\bar{\sigma}$	0.012	0.015	0.015	0.016
	QSN	$\bar{e}\bar{r}$	0.015	0.016	0.014	0.014
		$\bar{\sigma}$	0.011	0.012	0.010	0.010
	SW	$\bar{e}\bar{r}$	0.013	0.014	0.013	0.011
		$\bar{\sigma}$	0.009	0.010	0.008	0.008
60%	ER	$\bar{e}\bar{r}$	0.016	0.015	0.014	0.014
		$\bar{\sigma}$	0.012	0.011	0.009	0.008
	SF	$\bar{e}\bar{r}$	0.016	0.019	0.020	0.021
		$\bar{\sigma}$	0.012	0.014	0.015	0.015
	QSN	$\bar{e}\bar{r}$	0.015	0.015	0.013	0.013
		$\bar{\sigma}$	0.011	0.011	0.010	0.009
	SW	$\bar{e}\bar{r}$	0.013	0.015	0.012	0.011
		$\bar{\sigma}$	0.009	0.010	0.008	0.007
80%	ER	$\bar{e}\bar{r}$	0.016	0.014	0.013	0.011
		$\bar{\sigma}$	0.012	0.011	0.009	0.008
	SF	$\bar{e}\bar{r}$	0.016	0.019	0.021	0.021
		$\bar{\sigma}$	0.012	0.015	0.015	0.015
	QSN	$\bar{e}\bar{r}$	0.015	0.015	0.013	0.013
		$\bar{\sigma}$	0.011	0.011	0.010	0.009
	SW	$\bar{e}\bar{r}$	0.012	0.014	0.012	0.010
		$\bar{\sigma}$	0.009	0.009	0.008	0.007
Full(Raw)	ER	$\bar{e}\bar{r}$	0.016	0.015	0.012	0.010
		$\bar{\sigma}$	0.012	0.011	0.009	0.008
	SF	$\bar{e}\bar{r}$	0.016	0.019	0.021	0.021
		$\bar{\sigma}$	0.012	0.015	0.015	0.016
	QSN	$\bar{e}\bar{r}$	0.015	0.015	0.013	0.012
		$\bar{\sigma}$	0.011	0.011	0.009	0.008
	SW	$\bar{e}\bar{r}$	0.012	0.014	0.012	0.010
		$\bar{\sigma}$	0.009	0.009	0.008	0.007

For example, in SW networks with $\langle k \rangle = 10$, both 3-Hop and 4-Hop achieve the same mean error of 0.010 and standard deviation of 0.007. Since a larger K-value increases the computational complexity of constructing the hypergraph, choosing $K=4$ offers no significant accuracy benefit over $K=3$.

- **Consistent Improvement Over $K=2$** : While 3-Hop doesn't show a large advantage over 4-Hop, it does offer slight but consistent improvements over 2-Hop in several cases. For instance, in QSN networks with $\langle k \rangle = 10$, the mean error drops from 0.013 at 2-Hop to 0.012 at 3-Hop. This suggests that moving from $K=2$ to $K=3$ captures more valuable high-order information.
- **Identical Performance on SF Networks**: For SF networks, the performance is identical across all three K-values. In this scenario, selecting the lowest computationally

expensive option that still performs well on other network types (like $K=3$) is the most logical choice.

In summary, $K=3$ was likely chosen because it hits a sweet spot. It captures more complex network structures than $K=2$, leading to slightly better performance, while avoiding the increased computational cost of $K=4$, which provides no meaningful improvement in accuracy.

TABLE S3

THE MEAN ERROR ER AND MEAN STANDARD DEVIATION A OF THE CONTROLLED ROBUSTNESS CURVES OF NCR-HoK'S PREDICTION FOR DIFFERENT NETWORK TOPOLOGIES FOR K-HOP'S K-VALUES OF 2, 3, AND 4 CASES, RESPECTIVELY.

RA Attack		$\langle k \rangle=2$	$\langle k \rangle=5$	$\langle k \rangle=8$	$\langle k \rangle=10$	
2-Hop	ER	\bar{e}_r	0.016	0.014	0.012	0.011
		$\bar{\sigma}$	0.013	0.011	0.010	0.008
	SF	\bar{e}_r	0.016	0.019	0.021	0.021
		$\bar{\sigma}$	0.013	0.015	0.016	0.016
	QSN	\bar{e}_r	0.015	0.015	0.013	0.013
		$\bar{\sigma}$	0.011	0.011	0.010	0.009
SW	\bar{e}_r	0.012	0.015	0.012	0.010	
	$\bar{\sigma}$	0.009	0.010	0.009	0.008	
3-Hop (Raw)	ER	\bar{e}_r	0.016	0.015	0.012	0.010
		$\bar{\sigma}$	0.012	0.011	0.009	0.008
	SF	\bar{e}_r	0.016	0.019	0.021	0.021
		$\bar{\sigma}$	0.012	0.015	0.015	0.016
	QSN	\bar{e}_r	0.015	0.015	0.013	0.012
		$\bar{\sigma}$	0.011	0.011	0.009	0.008
SW	\bar{e}_r	0.012	0.014	0.012	0.010	
	$\bar{\sigma}$	0.009	0.009	0.008	0.007	
4-Hop	ER	\bar{e}_r	0.016	0.015	0.012	0.011
		$\bar{\sigma}$	0.012	0.011	0.009	0.008
	SF	\bar{e}_r	0.016	0.019	0.021	0.021
		$\bar{\sigma}$	0.012	0.015	0.016	0.016
	QSN	\bar{e}_r	0.015	0.014	0.013	0.013
		$\bar{\sigma}$	0.011	0.010	0.009	0.009
SW	\bar{e}_r	0.013	0.014	0.012	0.010	
	$\bar{\sigma}$	0.009	0.009	0.008	0.007	

2) K-NN Experiments on the different choice of K:

Based on the data in table S4, the choice of $K=10$ (10-NN) is a reasonable and justified default because the model's performance shows almost no sensitivity to the K-value in the K-NN hypergraph construction. As shown in the table results:

- **Consistent Performance Across All K-Values:** When comparing the results for 5-NN, 10-NN, 20-NN, and 30-NN, the mean error and standard deviation are remarkably stable across all network types and average degrees. For example:
 - For SF networks with an average degree of $\langle k \rangle = 8$, the mean error is consistently 0.021 and the standard deviation is 0.015, regardless of whether K is 5, 10, 20, or 30.
 - For SW networks with $\langle k \rangle = 10$, both the mean error (0.010) and standard deviation (0.007) are identical across all four K-NN settings.
- **No Advantage when Increasing K:** Unlike the K-Hop analysis where a larger K sometimes offered marginal benefits, here there is no discernible improvement from increasing K from 10 to 20 or 30. Since a larger K -value increases the density of the hypergraph and thus the computational cost, choosing a higher value offers no practical benefit.

In summary, because the model's prediction accuracy is insensitive to this specific hyperparameter, choosing $K=10$ serves as a sensible middle-ground. It's large enough to capture local neighborhood structures in the embedding space but not so large as to add unnecessary computational complexity for no performance gain.

TABLE S4

THE MEAN ERROR ER AND MEAN STANDARD DEVIATION A OF THE CONTROLLED ROBUSTNESS CURVES OF NCR-HoK'S PREDICTION FOR DIFFERENT NETWORK TOPOLOGIES FOR K-NN'S K-VALUES OF 5, 10, 20 AND 30 CASES, RESPECTIVELY.

RA Attack			$\langle k \rangle=2$	$\langle k \rangle=5$	$\langle k \rangle=8$	$\langle k \rangle=10$
5-NN	ER	\bar{e}_r	0.016	0.014	0.012	0.010
		$\bar{\sigma}$	0.012	0.011	0.009	0.008
	SF	\bar{e}_r	0.016	0.019	0.021	0.021
		$\bar{\sigma}$	0.012	0.015	0.016	0.015
	QSN	\bar{e}_r	0.015	0.014	0.013	0.012
		$\bar{\sigma}$	0.011	0.011	0.010	0.009
SW	\bar{e}_r	0.012	0.014	0.011	0.010	
	$\bar{\sigma}$	0.010	0.010	0.009	0.007	
10-NN (Raw)	ER	\bar{e}_r	0.016	0.015	0.012	0.010
		$\bar{\sigma}$	0.012	0.011	0.009	0.008
	SF	\bar{e}_r	0.016	0.019	0.021	0.021
		$\bar{\sigma}$	0.012	0.015	0.015	0.016
	QSN	\bar{e}_r	0.015	0.015	0.013	0.012
		$\bar{\sigma}$	0.011	0.011	0.009	0.008
SW	\bar{e}_r	0.012	0.014	0.012	0.010	
	$\bar{\sigma}$	0.009	0.009	0.008	0.007	
20-NN	ER	\bar{e}_r	0.016	0.014	0.013	0.012
		$\bar{\sigma}$	0.012	0.011	0.010	0.008
	SF	\bar{e}_r	0.016	0.019	0.021	0.021
		$\bar{\sigma}$	0.013	0.015	0.016	0.016
	QSN	\bar{e}_r	0.015	0.015	0.013	0.013
		$\bar{\sigma}$	0.011	0.011	0.010	0.009
SW	\bar{e}_r	0.012	0.015	0.012	0.011	
	$\bar{\sigma}$	0.009	0.010	0.008	0.008	
30-NN	ER	\bar{e}_r	0.016	0.015	0.012	0.010
		$\bar{\sigma}$	0.012	0.011	0.009	0.008
	SF	\bar{e}_r	0.016	0.019	0.021	0.021
		$\bar{\sigma}$	0.013	0.015	0.016	0.016
	QSN	\bar{e}_r	0.015	0.014	0.013	0.012
		$\bar{\sigma}$	0.011	0.011	0.010	0.009
SW	\bar{e}_r	0.013	0.014	0.012	0.010	
	$\bar{\sigma}$	0.009	0.010	0.009	0.007	

F. Analysis on More Different Attack Scenarios

We supplemented our analysis with Target Degree Based Attacks (TDA) and Target Betweenness Based Attacks (TBA) results. The experimental results, presented in tables S5 and S6, demonstrate that NCR-HoK maintains a significant advantage under both attack scenarios, further highlighting the robustness of our approach.

1) *Performance under TDA:* As shown in table S5, our model achieves the top rank (#1) in overall average performance for every network type (ER, SF, QSN, and SW) under Target Degree Based Attacks. For instance, on SF networks, NCR-HoK's average error is 0.010, which is substantially lower than the next best model, CRL-SGNN (0.035). Furthermore, our model consistently records the lowest average standard deviation, indicating that its predictions are not only accurate but also highly stable.

2) *Performance under TBA:* The results under Target Betweenness Based Attacks, detailed in table S6, reinforce this conclusion. Our model again secures the top rank (#1) for

overall average error on every network, where it still achieves a competitive first-place rank (#1).

TABLE S5

THE AVERAGE ERRORS \overline{eT} AND AVERAGE STANDARD DEVIATIONS $\overline{\sigma}$ OF THE CONTROLLABLE ROBUSTNESS CURVE PREDICTING FOR VARIOUS TYPES OF NETWORKS UNDER THE TDA CONDITION ARE COMPARED AMONG THE NCR-HoK, PCR [27], iPCR [28] MODELS AND CRL-SGNN [29], ALONG WITH A COMPREHENSIVE RANKING.

			<k>=2	<k>=5	<k>=8	<k>=10	Average
ER	PCR	\overline{eT}	0.039	0.040	0.018	0.013	0.028(#3)
		$\overline{\sigma}$	0.017	0.016	0.010	0.008	0.013(#2)
	iPCR	\overline{eT}	0.053	0.004	0.008	0.006	0.018(#2)
		$\overline{\sigma}$	0.070	0.004	0.007	0.006	0.022(#3)
	CRL-SGNN	\overline{eT}	0.013	0.070	0.019	0.049	0.038(#4)
		$\overline{\sigma}$	0.014	0.047	0.022	0.051	0.034(#4)
	Our	\overline{eT}	0.011	0.020	0.012	0.011	0.014(#1)
		$\overline{\sigma}$	0.007	0.011	0.007	0.007	0.008(#1)
SF	PCR	\overline{eT}	0.073	0.061	0.047	0.042	0.056(#4)
		$\overline{\sigma}$	0.004	0.008	0.009	0.010	0.008(#2)
	iPCR	\overline{eT}	0.010	0.182	0.012	0.008	0.053(#3)
		$\overline{\sigma}$	0.009	0.198	0.014	0.010	0.058(#4)
	CRL-SGNN	\overline{eT}	0.026	0.033	0.025	0.057	0.035(#2)
		$\overline{\sigma}$	0.032	0.049	0.035	0.082	0.050(#2)
	Our	\overline{eT}	0.005	0.010	0.011	0.013	0.010(#1)
		$\overline{\sigma}$	0.003	0.005	0.006	0.007	0.005(#1)
QSN	PCR	\overline{eT}	0.017	0.021	0.017	0.017	0.018(#2)
		$\overline{\sigma}$	0.007	0.011	0.010	0.010	0.010(#2)
	iPCR	\overline{eT}	0.009	0.114	0.011	0.008	0.036(#3)
		$\overline{\sigma}$	0.011	0.129	0.013	0.011	0.041(#4)
	CRL-SGNN	\overline{eT}	0.074	0.059	0.016	0.031	0.045(#4)
		$\overline{\sigma}$	0.026	0.073	0.020	0.037	0.039(#3)
	Our	\overline{eT}	0.010	0.018	0.014	0.014	0.014(#1)
		$\overline{\sigma}$	0.006	0.012	0.010	0.009	0.009(#1)
SW	PCR	\overline{eT}	0.010	0.011	0.012	0.011	0.011(#2)
		$\overline{\sigma}$	0.005	0.007	0.008	0.007	0.007(#2)
	iPCR	\overline{eT}	0.009	0.079	0.011	0.008	0.027(#3)
		$\overline{\sigma}$	0.013	0.093	0.014	0.012	0.033(#3)
	CRL-SGNN	\overline{eT}	0.023	0.047	0.033	0.029	0.033(#4)
		$\overline{\sigma}$	0.031	0.054	0.039	0.035	0.039(#4)
	Our	\overline{eT}	0.006	0.012	0.011	0.010	0.010(#1)
		$\overline{\sigma}$	0.004	0.007	0.007	0.007	0.006(#1)

TABLE S6

THE AVERAGE ERRORS \overline{eT} AND AVERAGE STANDARD DEVIATIONS $\overline{\sigma}$ OF THE CONTROLLABLE ROBUSTNESS CURVE PREDICTING FOR VARIOUS TYPES OF NETWORKS UNDER THE TBA CONDITION ARE COMPARED AMONG THE NCR-HoK, PCR [27], iPCR [28] MODELS AND CRL-SGNN [29], ALONG WITH A COMPREHENSIVE RANKING.

			<k>=2	<k>=5	<k>=8	<k>=10	Average
ER	PCR	\overline{eT}	0.047	0.033	0.018	0.016	0.029(#3)
		$\overline{\sigma}$	0.017	0.015	0.012	0.010	0.014(#2)
	iPCR	\overline{eT}	0.080	0.013	0.011	0.013	0.029(#3)
		$\overline{\sigma}$	0.086	0.009	0.011	0.013	0.030(#3)
	CRL-SGNN	\overline{eT}	0.014	0.041	0.015	0.038	0.027(#2)
		$\overline{\sigma}$	0.015	0.052	0.014	0.038	0.030(#3)
	Our	\overline{eT}	0.017	0.014	0.016	0.012	0.015(#1)
		$\overline{\sigma}$	0.012	0.010	0.010	0.009	0.010(#1)
SF	PCR	\overline{eT}	0.110	0.069	0.050	0.044	0.068(#4)
		$\overline{\sigma}$	0.014	0.017	0.015	0.015	0.015(#2)
	iPCR	\overline{eT}	0.014	0.180	0.013	0.013	0.055(#3)
		$\overline{\sigma}$	0.012	0.204	0.012	0.011	0.060(#4)
	CRL-SGNN	\overline{eT}	0.038	0.027	0.022	0.040	0.032(#2)
		$\overline{\sigma}$	0.042	0.030	0.021	0.042	0.034(#3)
	Our	\overline{eT}	0.010	0.014	0.014	0.013	0.013(#1)
		$\overline{\sigma}$	0.008	0.010	0.010	0.010	0.010(#1)
QSN	PCR	\overline{eT}	0.027	0.023	0.021	0.019	0.023(#2)
		$\overline{\sigma}$	0.012	0.012	0.013	0.012	0.012(#2)
	iPCR	\overline{eT}	0.017	0.127	0.014	0.014	0.043(#4)
		$\overline{\sigma}$	0.013	0.137	0.012	0.013	0.044(#4)
	CRL-SGNN	\overline{eT}	0.038	0.043	0.020	0.036	0.034(#3)
		$\overline{\sigma}$	0.041	0.051	0.025	0.042	0.040(#3)
	Our	\overline{eT}	0.014	0.015	0.014	0.013	0.014(#1)
		$\overline{\sigma}$	0.008	0.009	0.009	0.009	0.009(#1)
SW	PCR	\overline{eT}	0.014	0.021	0.018	0.016	0.017(#2)
		$\overline{\sigma}$	0.006	0.013	0.012	0.010	0.010(#1)
	iPCR	\overline{eT}	0.012	0.096	0.016	0.013	0.034(#4)
		$\overline{\sigma}$	0.013	0.099	0.015	0.013	0.035(#4)
	CRL-SGNN	\overline{eT}	0.015	0.037	0.034	0.040	0.032(#3)
		$\overline{\sigma}$	0.015	0.042	0.037	0.047	0.033(#3)
	Our	\overline{eT}	0.009	0.013	0.014	0.013	0.012(#1)
		$\overline{\sigma}$	0.004	0.013	0.014	0.013	0.011(#2)